Sigmoidal Water Retention Function with Improved Behavior in Dry and Wet Soils

Gerrit Huibert de Rooij, Juliane Mai, and Raneem Madi

G.H. de Rooij and R. Madi, Helmholtz Centre for Environmental Research – UFZ GmbH, Soil System Science Dept., Theodor–Lieser–Strasse 4, 06120 Halle (Saale), Germany; R. Madi, current address: GFI Grundwasser–Consulting–Institut GmbH, Meraner Strasse 10, 01217 Dresden, Germany.

J. Mai, University of Waterloo, Dept. Civil and Environmental Engineering, 200 University Ave West, Waterloo, ON N2L 3G1, Canada.

Corresponding author: G.H. de Rooij (gerrit.derooij@ufz.de)

Abstract

A popular parameterized soil water retention curve (SWRC) has a hydraulic conductivity curve associated with it that can have a physically unacceptable infinite slope at saturation. The problem was eliminated before by giving the SWRC a non–zero air–entry value. This improved version still has an asymptote at the dry end, which limits its usefulness for dry conditions and causes its integral to diverge for commonly occurring parameter values. We therefore joined the parameterizations' sigmoid mid–section to a logarithmic dry section ending at zero water content for a finite matric potential, as was done previously for a power–law type SWRC. We selected five SWRC parameterizations that had been proven to produce unproblematic near–saturation conductivities and fitted these and our new curve to data from 21 soils. The logarithmic dry branch gave more realistic extrapolations into the dry end of both the retention and the conductivity curves than an asymptotic dry branch. We tested the original curve, its first improvement, and our second improvement by feeding them into a numerical model that calculated evapotranspiration and deep drainage for nine combinations of soils and climates. The new curve was more robust than the other two. The new curve was better able to produce a conductivity curve with a substantial drop during the early stages of drying than the earlier improvement. It therefore generated smaller amounts of more evenly distributed deep drainage compared to the spiked response to rainfall produced by the earlier improvement.

Introduction

The soil water retention function introduced by van Genuchten (1980) has been the most popular parameterization (denoted VGN below; these and other abbreviations are listed in Appendix A) to describe the SWRC in numerical models for unsaturated flow for the past few decades (e.g., Kroes et al., 2017; Šimůnek and Bradford, 2008; Šimůnek et al., 2016):

$$\theta(h) = \theta_r + (\theta_s - \theta_r)(1 + |\alpha h|^n)^{\frac{1}{n}-1}, \quad h \leq 0 \qquad (1)$$

where h denotes the matric potential in equivalent water column [L]. The volumetric water content is denoted by θ, with the subscript 's' denoting its value at saturation and the subscript 'r' its residual, or irreducible, value. Parameters α [L^{-1}] and n are shape parameters.

Van Genuchten (1980) combined Eq. (1) with Mualem's (1976) conductivity model and derived an analytical expression for the unsaturated hydraulic conductivity curve:

$$K(h) = K_s \frac{\left[1 - |\alpha h|^{n-1}(1+|\alpha h|^n)^{\frac{1}{n}-1}\right]^2}{(1+|\alpha h|^n)^{\frac{1}{2}-\frac{1}{2n}}} \qquad (2)$$

where K[LT^{-1}] is the soil hydraulic conductivity and K_s [LT^{-1}] its value at saturation.

Hysteretic (Kool and Parker, 1987) and multimodal versions (Durner, 1994) of Eq. (1) are available. Apart from the convenience of having analytical expressions for the retention as well as the conductivity curve, the function's popularity derives from its

continuous derivative and its inflection point, which gives it considerable flexibility in fitting observations.

~~Fuentes et al. (1991) warned that the asymptotic residual water content at the dry end could lead to a non–converging integral of the retention curve, and showed how this would mathematically lead to a physically impossible unlimited water uptake capacity of a finite soil column. From their analysis follows that this can only be prevented if $n > 2$ in Eq. (1), a condition which is often not satisfied.~~

Fuentes et al. (1991) warned that the asymptotic residual water content at the dry end could lead to a non–converging integral of the retention curve when the integration is carried out between the saturated water content and a water content that approximates the residual water content in the limit. In that case, the area below the retention curve becomes infinite. Fuentes et al. (1991) showed that this would lead to an unlimited amount of water stored in a column of a finite length at hydrostatic equilibrium if its height was such that the residual water content was approximated closely at the top of the column. This physically impossible case is only avoided if $n > 2$ in Eq. (1), a condition which is often not satisfied.

Near saturation, the slope $\mathrm{d}\theta/\mathrm{d}h$ is not zero at zero matric potential. This implies that the soil has pores that have at least one infinite principal radius according to the Laplace–Young Law (Hillel, 1998, p. 46), which is physically unacceptable (see also Iden et al., 2015). Durner (1994) noted this could lead to an infinite slope in the hydraulic conductivity function of Mualem (1976) when the matric potential approached zero, and Ippisch et al. (2006) showed that if $n < 2$ this would indeed be the case. The more recent sigmoid curve of Fredlund and Xing (1994) and its modification by Wang et al. (2016), used by Wang et al. (2018) and Rudiyanto et al. (2020) have the same problem (see Appendix B

for the proof). The curve of Assouline et al. (1998) is based on the Weibull distribution, and therefore has a non–zero slope at zero matric potential when its fitting parameter η is smaller than 2, which was the case for 75% of the soils for which it was fitted. None of these curves therefore offers a remedy to the problem associated with VGN.

Corrections for the conductivity curve were proposed by Vogel et al. (2001), Schaap and van Genuchten (2006), and Iden et al. (2015), but these leave the effect of the non–physical, very large pores on the SWRC intact and create an inconsistency between the retention model and the conductivity model. For instance, Iden et al. (2015) clipped the integral in the conductivity function at a matric potential h_c somewhat below zero. In the range between h_c and zero, their modified unsaturated hydraulic conductivity increased linearly with the water content (Iden et al. (2015), Fig. 1), which is not physically realistic because the pore sizes that are being filled are increasing in size according to Eq. (1) or its multimodal version (Peters et al., 2011). Only Ippisch et al. (2006) addressed the underlying problem in the SWRC by introducing a non–zero air–entry value, thereby eliminating excessively large pores whilst maintaining the mathematical consistency between the expressions for the retention and the conductivity curves. In doing so they sacrificed the continuity of the derivative of the VGN curve. Iden et al. (2015) suspected this would pose a challenge to numerical solves of Richards' equation, but Ippisch et al.'s (2006) numerical simulations ran without difficulty. Their equation scaled the sigmoid curve by its value at the air–entry value h_{ae} [L] and introduced a saturated section for $h > h_{ae}$.

$$\theta(h) = \begin{cases} \theta_r + (\theta_s - \theta_r)\left(\frac{1+|\alpha h|^n}{1+|\alpha h_{ae}|^n}\right)^{\frac{1}{n}-1}, & h \le h_{ae} \\ \theta_s, & h > h_{ae} \end{cases} \quad (3)$$

This function is denoted VGA below.

The smooth, sigmoidal shape of VGN resembles many observed curves for which the data points in the wet range were obtained by equilibrating vertically placed cylindrical soil samples at well–defined matric potentials and determining the corresponding water content by weighing the sample (Klute, 1986, p. 644–647). Liu and Dane (1995) took into account the vertical variation of the water content in such samples and demonstrated that a power–law SWRC with a well–defined air–entry matric value but without inflection point can produce a sigmoid–type apparent SWRC if the non–uniform distribution of water in the sample is ignored. A series of data points suggesting a smooth SWRC therefore does not intrinsically contradict the existence of a discrete non–zero air–entry value, corroborating the correction to VGN by Ippisch et al. (2006).

In a separate development, several researchers argued that in the dry range, water is bound to the soil by adsorptive rather than capillary forces. Usually, a logarithmic term that allowed the adsorbed water content to go to zero at a prescribed matric potential was added to a capillary term. The former would dominate in the dry range and become negligible as the soil became wetter (e.g., Campbell and Shiozawa, 1992; Fayer and Simmons, 1995; Khlosi et al., 2006; Peters, 2013). The logarithmic relationship was based on the sorption theory of Bradley (1936). It removed the asymptote and the associated problem of the non–converging integral of the SWRC that Fuentes et al. (1991) warned about. Rossi and Nimmo (1994) presented a junction model in which a critical matric potential separated purely capillary bound water ~~(described by a variation of the Brooks–~~

~~Corey (1964) model)~~ from solely adsorbed water. The junction model of Rossi and Nimmo (1994) is

$$\theta(h) = \begin{cases} \theta_s \beta \mathit{ln}\left(\frac{h_d}{h}\right), & h_d \le h \le h_j \\ \theta_s \left(\frac{h_0}{h}\right)^{\lambda}, & h_j \le h \le h_i \\ \theta_s \left[1 - c\left(\frac{h}{h_0}\right)^2\right], & h_i \le h \le 0 \end{cases} \quad (4)$$

The first (dry) branch is logarithmic, with h_d [L] the matric potential at which the water content reaches zero, and β a shape parameter. The middle branch is the power law adopted from Brooks and Corey (1964), where λ is a shape parameter and h_0 [L] is a fitting parameter. The final (wet) branch is a parabolic correction to avoid a discontinuity in the derivative at the air-entry value, with parameter c a function of λ and h_0 (Hutson and Cass, 1987). Madi et al. (2018) pointed out that this correction puts such strict constraints on the parameters of the conductivity curve that the usual models are ruled out. The first and middle branch are joined at h_j [L], the middle and final branch at h_i [L]. Rossi and Nimmo (1994) reduced the number of fitting parameters by requiring that the water contents and the first derivatives of the branches match at at h_j and h_i.

~~By doing so they avoided~~ This junction model avoids the problem of many of the other models that would have some capillary bound water still present in the soil below the matric potential at which the adsorbed water content had gone to zero.

Madi et al. (2018) generalized the analysis of Ippisch et al. (2006) and applied it to 18 parameterizations of the SWRC to verify that the slope of the hydraulic conductivity near saturation would remain finite. Apart from Eq. (3), only the expressions developed by

144 Brooks and Corey (1964) (denoted BCO), Fayer and Simmons (1995) (denoted FSB), and
145 the junction model of Rossi and Nimmo (1994) (denoted RNA) satisfied this requirement.
146 In the latter case, Eq. (4) had to be modified by removing a modification that smoothed the
147 curve near saturation. All these equations have a power law relationship between the water
148 content and the matric potential, and therefore do not have the sigmoid shape of VGN and
149 VGA.

150 As noted above, the introduction of a non–zero air–entry value by Ippisch et al.
151 (2006) eliminated the unphysically large slopes of the hydraulic conductivity according to
152 Mualem (1976). The approach of Rossi and Nimmo (1994) resolved the issue of the
153 asymptotic behavior in the dry range. The objective of this paper therefore is to combine
154 Rossi and Nimmo's (1994) model for the dry range with the VGA model of Ippisch et al.
155 (2006) to arrive at a SWRC (denoted RIA) that has a non–zero air–entry value, a sigmoid
156 shape in the intermediate range, a dry branch that can reach zero water content at a finite
157 matric potential, and therefore a finite integral. We will also develop a closed-form
158 expression for the unsaturated hydraulic conductivity based on this SWRC. For
159 completeness, a generalized expression for multimodal SWRCs will also be derived.

160 Together with the other functions that lead to physically acceptable behavior of the
161 hydraulic conductivity near saturation (BCO, FSB, RNA, and VGA), RIA will be fitted to 21
162 soils selected from the UNSODA database (National Agricultural Library, 2017; Nemes et al.,
163 2001) that cover a wide range of textures (Madi et al., 2018). For comparison VGN is also
164 included, in view of its de facto status as the standard parameterization for the SWRC. All
165 three versions with the sigmoid shape (VGN, VGA, and RIA) will be tested in a simulation
166 study for different combinations of soil types and climates.

Theory

The Soil Water Retention Curve

The junction model of Rossi and Nimmo (1994) has a SWRC with a logarithmic dry branch without residual water content. The parameterization proposed by Ippisch et al. (2006) combines the sigmoid shape of van Genuchten (1980) with a non–zero air–entry value. By setting the θ_r in Ippisch et al. (2006) to zero, we can combine the two models to give the following parameterization:

$$\theta(h) = \begin{cases} 0, & h \le h_\mathrm{d} \\ \theta_\mathrm{s}\beta \ln\left(\frac{h_\mathrm{d}}{h}\right), & h_\mathrm{d} < h \le h_\mathrm{j} \\ \theta_\mathrm{s}\left(\frac{1+|\alpha h|^n}{1+|\alpha h_\mathrm{ae}|^n}\right)^{\frac{1}{n}-1}, & h_\mathrm{j} < h \le h_\mathrm{ae} \\ \theta_\mathrm{s}, & h > h_\mathrm{ae} \end{cases} \quad (5)$$

where subscripts ‘d’ and ‘ae’ denote the value at which the water content reaches zero and the air–entry value, respectively, and subscript ‘j’ indicates the value at which the logarithmic and sigmoid branch are joined. The first branch ensures that no water can be present at matric potentials below h_d. The second, logarithmic, branch is identical to that of Eq. (4). The third, sigmoidal, branch between h_j and h_ae, and the fourth branch, for matric potentials larger than the air-entry value, are from Eq. (3). Joining instead of adding the logarithmic and the sigmoid functions avoids potentially non-monotonic behavior (Peters et al., 2011).

The derivative of Eq. (5) is

$$\frac{\mathrm{d}\theta}{\mathrm{d}h}(h) = \begin{cases} 0, & h \le h_{\mathrm{d}} \\ \frac{\theta_{\mathrm{s}}\beta}{h}, & h_{\mathrm{d}} < h \le h_{\mathrm{j}} \\ \theta_{\mathrm{s}}\alpha(n-1)|\alpha h|^{n-1}(1+|\alpha h_{\mathrm{ae}}|^n)^{1-\frac{1}{n}}(1+|\alpha h|^n)^{\frac{1}{n}-2}, & h_{\mathrm{j}} < h \le h_{\mathrm{ae}} \\ 0, & h > h_{\mathrm{ae}} \end{cases} \quad (6)$$

Mass continuity dictates that the SWRC is continuous. At the air–entry value, this condition is met irrespective of the parameter values. At h_{j}, continuity requires the following equality to hold:

$$\beta \ln\left(\frac{h_{\mathrm{d}}}{h_{\mathrm{j}}}\right) = \left(\frac{1+|\alpha h_{\mathrm{j}}|^n}{1+|\alpha h_{\mathrm{ae}}|^n}\right)^{\frac{1}{n}-1} \quad (7)$$

In accordance with Rossi and Nimmo (1994) we also require the derivatives at h_{j} to match, leading to

$$\beta = (n-1)\left|\alpha h_{\mathrm{j}}\right|^n (1+|\alpha h_{\mathrm{ae}}|^n)^{1-\frac{1}{n}}\left(1+\left|\alpha h_{\mathrm{j}}\right|^n\right)^{\frac{1}{n}-2} \quad (8)$$

Combining Eqs. (7) and (8) and solving for h_{d} gives:

$$h_{\mathrm{d}} = h_{\mathrm{j}} \exp\left(\frac{1+|\alpha h_{\mathrm{j}}|^{-n}}{n-1}\right) \quad (9)$$

This leaves h_{ae}, h_{j}, θ_{s}, α, and n as fitting parameters.

The derivation of a multimodal curve analogous to that of Durner (1994) and Zurmühl and Durner (1998) is straightforward if the values of h_{ae} and h_j are kept the same for all contributing terms:

$$\theta(h) = \begin{cases} 0, & h \le h_d \\ \theta_s \beta \ln\left(\frac{h_d}{h}\right), & h_d < h \le h_j \\ \theta_s \sum_{i=1}^{k} w_i \left(\frac{1+|\alpha_i h|^{n_i}}{1+|\alpha_i h_{ae}|^{n_i}}\right)^{\frac{1}{n_i}-1}, & h_j < h \le h_{ae} \\ \theta_s, & h > h_{ae} \end{cases} \quad (10)$$

where the modality is indicated by k. The weighting factors w_i are bounded on the interval [0,1] and their sum must equal 1 (Durner, 1994; Zurmühl and Durner, 1998). Requiring the logarithmic and the multimodal branch as well as their derivatives to match at h_j leads to

$$\beta = \sum_{i=1}^{k} w_i (n_i - 1)\left|\alpha_i h_j\right|^{n_i} (1 + |\alpha_i h_{ae}|^{n_i})^{1-\frac{1}{n_i}} \left(1 + \left|\alpha_i h_j\right|^{n_i}\right)^{\frac{1}{n_i}-2} \quad (11)$$

and

$$h_d = h_j \exp\left[\frac{\sum_{i=1}^{k} w_i (1+|\alpha_i h_{ae}|^{n_i})^{1-\frac{1}{n_i}} \left(1+|\alpha_i h_j|^{n_i}\right)^{\frac{1}{n_i}-1}}{\sum_{i=1}^{k} w_i (n_i-1)|\alpha_i h_j|^{n_i} (1+|\alpha_i h_{ae}|^{n_i})^{1-\frac{1}{n_i}} \left(1+|\alpha_i h_j|^{n_i}\right)^{\frac{1}{n_i}-2}}\right] \quad (12)$$

The fitting parameters are h_{ae}, h_j, θ_s, α_i, n_i, and w_i.

The Unsaturated Hydraulic Conductivity Curve

The primary focus of this paper is on the SWRC. Nevertheless, it is worthwhile to find a closed-form expression for the unsaturated hydraulic conductivity that can be used in association with Eq. (5). Kosugi (1999) proposed the following conductivity model (see also Ippisch et al., 2006):

$$K(h) = K\big(h(S_e)\big) = \begin{cases} K_s S_e^{\tau} \left(\dfrac{\int_{-\infty}^{h(S_e)} |h|^{-\kappa} \frac{dS}{dh} dh}{\int_{-\infty}^{h_{ae}} |h|^{-\kappa} \frac{dS}{dh} dh} \right)^{\gamma}, & h < h_{ae} \\ K_s, & h \geq h_{ae} \end{cases} \tag{13}$$

with γ, κ, and τ denoting shape parameters, S_e denoting the degree of saturation, and S representing a variable running over all values of the degree of saturation from zero to its actual value S_e. Mualem's (1976) conductivity model is a special case of Eq. (12), with $\gamma = 2$, $\kappa = 1$, and $\tau = 0.5$. Madi et al. (2018) give parameter combinations for additional models.

The integrals in Eq. (13) that arise when Eq. (6) is used to find dS/dh can be evaluated analytically if $\kappa = 1$. The resulting conductivity function is

$$K(h) = \begin{cases} 0, & h \le h_{\mathrm{d}} \\ K_{\mathrm{s}}\left(\beta \ln\left|\frac{h_{\mathrm{d}}}{h}\right|\right)^{\tau}\left[\dfrac{\frac{\beta}{|h_{\mathrm{d}}|}-\frac{\beta}{|h|}}{\frac{\beta}{|h_{\mathrm{d}}|}-\frac{\beta}{|h_{\mathrm{j}}|}+\frac{|\alpha h_{\mathrm{ae}}|^{n}}{|h_{\mathrm{ae}}|}-(1+|\alpha h_{\mathrm{ae}}|^{n})^{1-\frac{1}{n}}F(h_{\mathrm{j}})}\right]^{\gamma}, & h_{\mathrm{d}} < h \le h_{\mathrm{j}} \\ K_{\mathrm{s}}\left(\dfrac{1+|\alpha h|^{n}}{1+|\alpha h_{\mathrm{ae}}|^{n}}\right)^{\frac{\tau}{n}-\tau}\left\{\dfrac{\frac{\beta}{|h_{\mathrm{d}}|}-\frac{\beta}{|h_{\mathrm{j}}|}+(1+|\alpha h_{\mathrm{ae}}|^{n})^{1-\frac{1}{n}}[F(h)-F(h_{\mathrm{j}})]}{\frac{\beta}{|h_{\mathrm{d}}|}-\frac{\beta}{|h_{\mathrm{j}}|}+\frac{|\alpha h_{\mathrm{ae}}|^{n}}{|h_{\mathrm{ae}}|}-(1+|\alpha h_{\mathrm{ae}}|^{n})^{1-\frac{1}{n}}F(h_{\mathrm{j}})}\right\}^{\gamma}, & h_{\mathrm{j}} < h \le h_{\mathrm{ae}} \\ K_{\mathrm{s}}, & h > h_{\mathrm{ae}} \end{cases} \tag{14a}$$

where

$$F(h) = \frac{|\alpha h|^{n}(1+|\alpha h|^{n})^{\frac{1}{n}-1}}{|h|} \tag{14b}$$

If only the hydraulic conductivity at saturation is available, one can use the values for α and n of the water retention curve and fix parameters γ and τ according to one of several conductivity models (Madi et al., 2018) to define an unsaturated hydraulic conductivity curve, but this is not recommended. It is better to have additional data points of the hydraulic conductivity curve so that parameters γ and τ, and perhaps even conductivity-specific values of α and n, can be fitted directly to the conductivity data.

Equations (14a) and (14b) have the advantage that they can be expressed in closed form but they do not account for non-capillary flow in dry soils, vapor flow, or sequences of

253 evaporation and condensation in soils with pockets of water and soil air. Hence, they are of
254 limited value for water flows in dry soils. For such conditions more sophisticated
255 conductivity could be selected, for instance using the framework presented by Weber et al.
256 (2019).
257 ~~Other conductivity models are available and can be selected if desired, for instance using~~
258 ~~the framework presented by Weber et al. (2019).~~
259 The conductivity function associated with the multimodal soil water retention
260 function cannot be expressed in closed form. For that case, the degree of saturation for any
261 h can be found with Eq. (10) and the corresponding hydraulic conductivity determined with
262 Eq. (13) or another conductivity model.
263

264 ## Materials and Methods

265 We selected 21 soils from the UNSODA database that had sufficient retention data
266 and together covered the textures represented in UNSODA. We then fitted Eq. (5) to these
267 soils using a Shuffled Complex Evolution algorithm (see Madi et al. (2018) and Appendix C
268 for details of the algorithm and the fitting procedure). We slightly modified the fitting code
269 used by Madi et al. (2018) to generate output that can more readily be converted to the
270 MATER.IN input file for Hydrus–1D, the numerical model used in this study. We therefore
271 refitted BCO, FSB, RNA, VGN, and VGA as well.
272 One–dimensional simulations for all combinations of three soils and three climates
273 were carried out to examine how the choice of parameterization affected fluxes at the soil
274 surface and in the subsoil. The model Hydrus–1D version 4.16.0110 (Šimůnek et al., 2013,
275 PC-progress website) was used for this purpose. The selected soils were a loamy sand

(UNSODA identifier: 2104), a silty loam (3261), and a clay (1181). Weather records were generated from climate parameters based on weather data from Colombo (Sri Lanka, monsoon climate), Tamale (Ghana, semi–arid climate), and Ukkel (Belgium, temperate climate). Table 1 gives the most relevant statistics of the weather records. In order to highlight the effects of the air–entry value and the logarithmic dry end of the SWRC, we used the sigmoidal VGN, VGA, and RIA parameterizations in the simulations. The Supplement details the generation of the weather records, the set–up of the simulations, and the simulation results.

285 Table 1. Average cumulative monthly and annual rainfall and potential evapotranspiration
286 of the three test climates calculated from 1000–year generated weather records.

	Monsoon		Semi–arid		Temperate	
Month	Rain (mm)	ET_{pot} (mm)	Rain (mm)	ET_{pot} (mm)	Rain (mm)	ET_{pot} (mm)
Jan	94.0	160.5	14.3	159.4	69.0	12.7
Feb	83.3	156.0	12.9	158.1	55.6	18.8
Mar	217.6	166.8	13.7	185.0	59.4	34.4
Apr	233.8	160.0	34.1	177.7	57.1	51.1
May	237.4	164.0	117.6	166.6	24.5	73.9
Jun	138.5	164.7	140.9	151.4	24.4	83.3
Jul	139.4	172.4	141.8	153.2	23.2	86.3
Aug	137.1	174.4	213.5	145.0	20.9	73.7
Sep	133.0	164.7	214.7	136.9	23.8	50.6
Oct	325.8	142.3	76.6	154.1	38.0	30.8
Nov	328.8	128.1	12.9	149.3	49.1	16.1
Dec	112.0	150.9	12.9	151.9	51.2	11.2
Annual sum	2180.5	1904.8	1005.8	1888.7	496.1	542.9

287

288

289

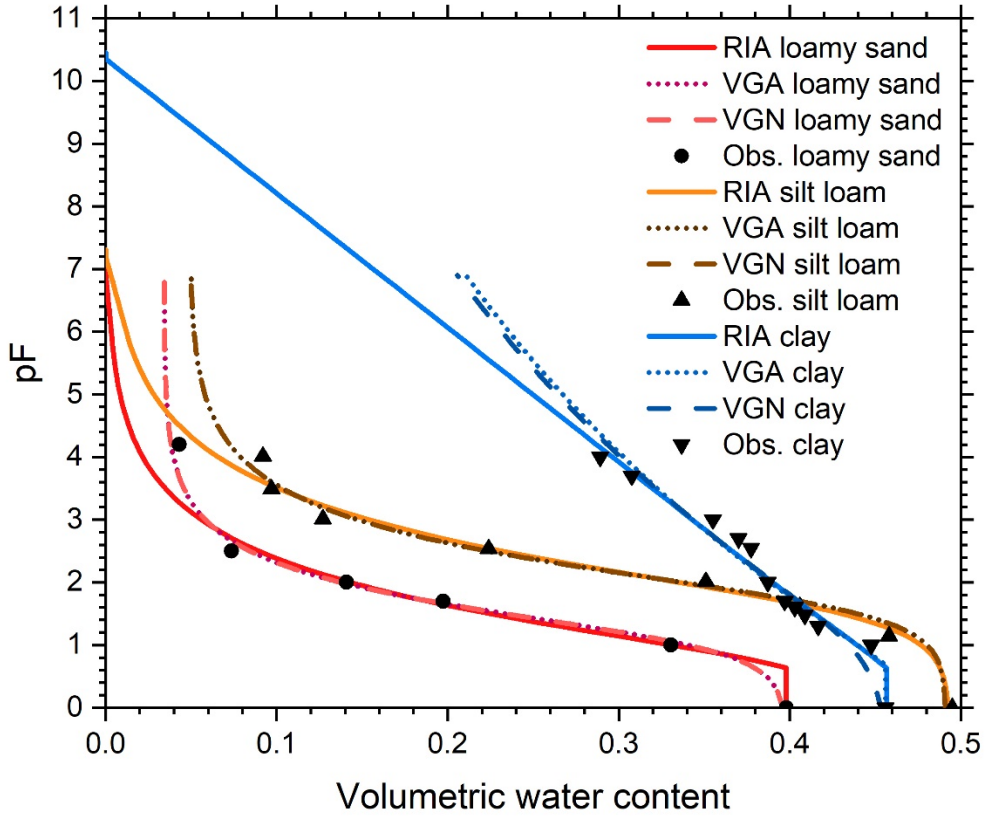

Figure 1. Soil water retention data of the soils used in the numerical simulations, and the retention curves fitted to these data for three parameterizations with a sigmoid midsection of the curve: the original model by van Genuchten (1980) (VGN), the modification thereof by Ippisch et al. (2006) (VGA), and the further modification introduced in this paper (RIA).

The different parameterizations of the SWRCs (Table 2, Fig. 1) were used to generate tables of the soil water retention and conductivity curves that were provided as input to Hydrus–1D. Mualem's (1976) model for the unsaturated soil hydraulic conductivity was used to generate relative hydraulic conductivities (scaled by K_s). These were converted to

unscaled conductivities (Fig. 2) by multiplying with the K_s–value according to the UNSODA database, and then included in the tables.

Table 2. Parameters of the fit to data of the three parameterizations of the soil water retention curve used for the numerical simulations.

Soil	Parameter	θ_r	θ_s	α (cm^{-1})	n	h_{ae} (cm)	h_j (cm)
Clay	RIA	–	0.45666	0.70200	1.0543	–4.2523	–205.65
	VGA	2.12×10^{-6}	0.45603	1.7047	1.0543	–4.8324	–
	VGN	3.34×10^{-6}	0.45616	0.14265	1.0571	–	–
Silt loam	RIA	–	0.49346	0.023340	1.3691	-2.361×10^{-3}	-1.0739×10^{6}
	VGA	0.048871	0.49122	0.018365	1.5158	-2.081×10^{-3}	–
	VGN	0.048816	0.49134	0.018425	1.5149	–	–
Loamy sand	RIA	–	0.39801	0.17096	1.4106	–4.3581	-7.7464×10^{5}
	VGA	0.034209	0.39771	0.069661	1.6395	–0.016234	–
	VGN	0.034133	0.39772	0.069707	1.6389	–	–

For the clay soil, the recorded value (178 cm d^{-1}) was such that it can be assumed that macropore flow contributed to its value. We therefore also ran simulations with a K_s – value of 1.25 cm d^{-1}. This value was adopted from soil 1182 from the UNSODA database, from the same location.

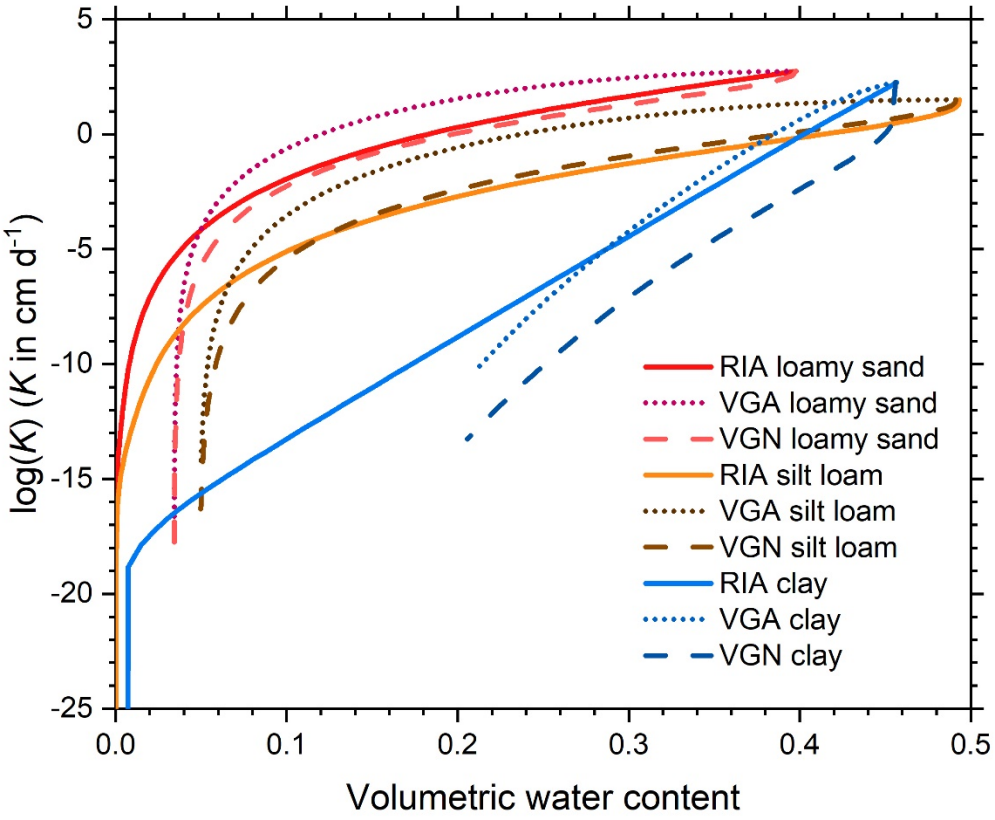

Figure 2. The unsaturated soil hydraulic conductivity curves derived from the fitted retention curves depicted in Fig.1 and scaled by soil–specific values of the hydraulic conductivity at saturation.

Results and Discussion

Fitted Curves for 21 Soils

The fitted parameter values (Tables C1–C4) and the associated curves (Figs. C2–C5) are presented in Appendix C. The extra parameter of RIA compared to RNA and FSB gives it a clear advantage in fitting the full water content range. The sigmoid shape of RIA provides

322 a better fit near the air entry value while still providing good fits of the drier data points
323 (e.g. 1121 in Fig. C3, all soils in Figs. C4–C5). In the wet range, the sigmoid curves (VGN,
324 VGA, RIA) outperform the power–law curves (BCO, FSB, RNA). In almost all cases, VGA and
325 RIA look very similar. Figure C3 shows multimodality in the data for five out of six soils that
326 cannot be reproduced by any of the parameterizations.
327 Many of the UNSODA soils have one retention data point at saturation and the next
328 at $h = -10$ cm. The air–entry value of many sandy soils is within that range. The fitting
329 routine struggles to fit h_{ae} to these data for VGA and RIA because the sigmoid shape of the
330 van Genuchten parameterization has such flexibility that it can fit the intermediate range
331 well for a range of h_{ae}–values. We therefore recommend making $\theta(h)$–measurements at one
332 or two matric potentials between zero and −10 cm for coarse–textured soils.
333 Eleven of the 21 soils have residual water contents for VGN and/or VGA that exceed
334 0.05 (up to 0.263), mostly in loamy sands, loams, and clays (Tables C1–C4). All of these and
335 several others have dry–end data points with water contents that appear too high (Figs. C2–
336 C5). These water contents may have been overestimated due to the lack of equilibrium
337 reported by Bittelli and Flury (2009). The parameterizations without asymptote (FSB, RNA,
338 RIA) generally have more plausible fits based on visual inspection of the graphs, but
339 because they do not follow the upward tail of the data in the dry end, their RMSE values for
340 the cases with suspicious dry–end data points are larger than those of VGN and VGA (Tables
341 C5–C8).
342 Especially for fine–textured soils, the lack of data points for air dryness or oven
343 dryness (Figs. C3–C5) causes the fitting procedure to treat θ_r for the asymptotic dry
344 branches and h_d for the logarithmic dry branches as pure fitting parameters for the drier

345 range of the data. This range exceeds pF4.2 in only one case and in several cases likely
346 suffers from lack of equilibrium (Bittelli and Flury, 2009). This leads to unrealistically high
347 values for both in many cases. If applications are envisioned for which low water contents
348 are expected, it would be better to have some data in the dry range and ensure equilibrium
349 has been achieved before fitting RIA.

350 We tested this on the data of Bittelli and Flury (2009) for undisturbed samples taken
351 at 0.15 m depth. We fitted RIA, VGA, and VGN with θ_s fixed at 0.45 to their pressure plate
352 data (which were unreliable in the dry range) and a combination of pressure plate data for
353 matric potentials larger than –1000 cm H_2O (pF3.0) and dew point data for higher pF
354 values (Table 3). Figure 3 shows that all three parameterizations gave good fits for both
355 data sets, and that the dry-end data points affect the entire SWRC. It is important to note
356 that the pF value of h_d for the combination of pressure plate and dew point data equals
357 6.428, close to the oven-dry value of pF6.8 approximated by most sample-drying ovens
358 according to Schneider and Goss (2012).

359 If reliable data in the dry range are not available but a realistic fit in the dry range is
360 necessary, one could add a virtual data point with zero water content at pF6.8 according to
361 Schneider and Goss (2012) and give it a high weight to force the fitting algorithm to
362 approximate it closely. We did not do so here to be able to observe how the various
363 parameterizations perform on frequently reported data ranges.

364 Figure C5 showcases a peculiarity of FSB. The original version by Fayer and
365 Simmons (1995) allowed capillary bound water to be present even if the adsorbed water
366 content was down to zero. We adopted the correction by Madi et al. (2018, Eq. (S12a)) that
367 forced the amount of water bound by capillary forces to zero if the adsorbed water content

368 reaches zero at pF6.8. In the case of clay soils, the parameter values are such that a
369 substantial amount of capillary bound water is still present at pF6.8, leading to a sudden
370 cut–off at pF6.8.
371
372 Table 3. Parameters of the fit to the pressure plate data and a combination of pressure plate
373 and dew point data of Bittelli and Flury (2009).

Data	Parameter	θ_r	θ_s	α (cm^{-1})	n	h_{ae} (cm)	h_j (cm)
Pressure plate	RIA	–	0.45000	0.019088	1.1479	-1.072×10^{-4}	–47876
	VGA	2.21×10^{-5}	0.45000	0.019091	1.1479	-3.105×10^{-3}	–
	VGN	6.76×10^{-7}	0.45000	0.019124	1.1478	–	–
Pressure plate (pF < 3) and dew point (pF ≥ 3)	RIA	–	0.45000	7.1162×10^{-3}	1.3041	-1.063×10^{-3}	–99989
	VGA	5.08×10^{-6}	0.45000	7.0471×10^{-3}	1.3056	-4.249×10^{-3}	–
	VGN	1.37×10^{-6}	0.45000	7.0448×10^{-3}	1.3053	–	–

374
375

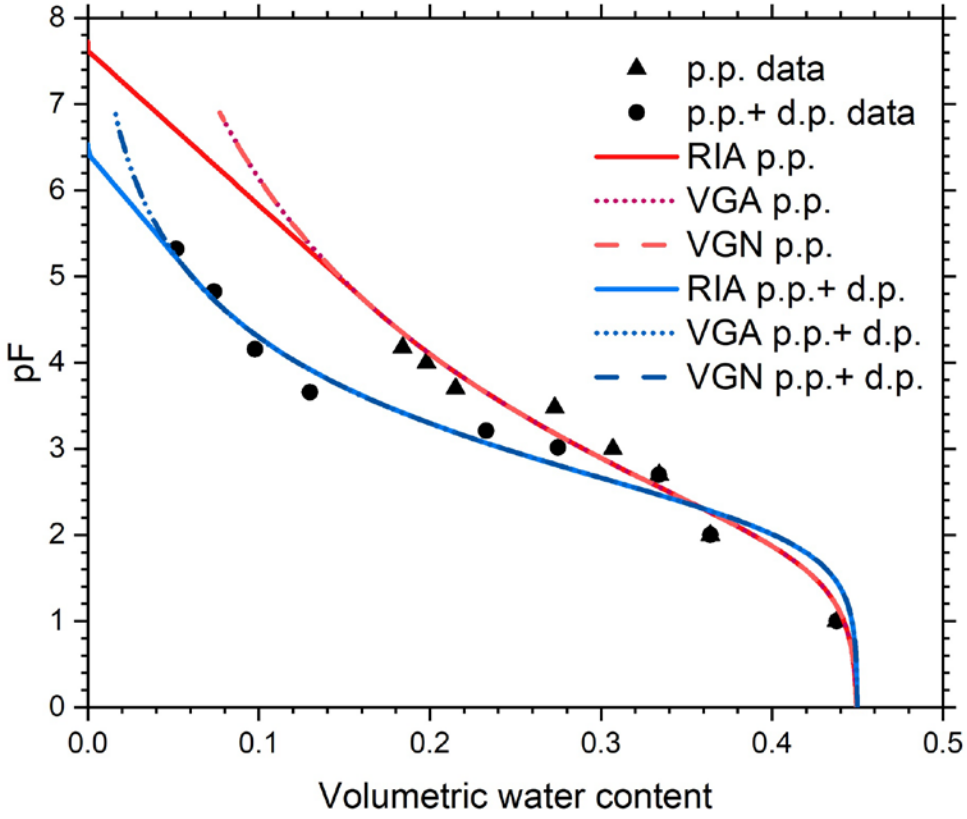

376

377 Figure 3. Soil water retention data obtained by Bittelli and Flury (2009) from samples
378 placed on pressure plates (p.p. data) or from a combination of pressure plates for the
379 wettest three data points and dew point measurements for the driest six data points (p.p. +
380 d.p. data). The curves show the fits of the soil water retention curves according to van
381 Genuchten (1989) (VGN), Ippisch et al. (2006) (VGA), and Eq. (5) (RIA).

382

383 The hydraulic conductivity curves based on water retention curve parameters and
384 K_s very poorly match the data in most cases (Fig. C6–C9), which confirms that it is better to
385 fit conductivity parameters to conductivity data instead of relying on values prescribed by
386 theoretical models. We note here that all but one (soil 4450, Fig. C8) sets of unsaturated

conductivity data were obtained in the field, while all retention data were laboratory data on drying samples. The reported K_s–values were probably measured in a separate experiment (possibly in the laboratory), in which case a mismatch between K_s and the unsaturated conductivity data is to be expected. The poor match with field data notwithstanding, the graphs can be used to study the effect of the parameterization on the shape of the $K(\theta)$ curve. The comparison between measured and modeled shapes of the conductivity curves is inconclusive.

In many soils, regardless of texture, RIA's $K(\theta)$ curve drops of much slower in the dry range than those of VGN and VGA (Fig. C6–C9), a consequence of the ability of the underlying SWRC to reach zero water content at a finite matric potential. Near saturation, RIA's $K(\theta)$ curve often drops off sharply before leveling off, in stark contrast to that of VGA, which remains high in the wet range. Given the similarity in the $\theta(h)$ curves of VGA and RIA, the difference in their $K(\theta)$ curves is remarkable. RIA's $K(\theta)$ curve is the only one that can drop off sharply near saturation, level out somewhat in the mid-range and drop ever more sharply in the dry range. It is below many of the other curves in the wet and mid-range, and above most of them in the dry range.

Peters et al. (2011) developed parameter constraints to ensure physically plausible shapes of the SRWC and the conductivity curve. For FSB, the criterion for non-monotonicity of the conductivity curve is not met for soil 4450 (Fig. C8), resulting in K increasing with decreasing water content near saturation.

Model Simulations

409 In total, 21 out of 36 combinations of soil–climate–parameterization ran to
410 completion. Runoff did not occur in any of the successful model runs. Convergence was not
411 achieved for any of the runs for the clay soil with the reduced K_s–value. For the clay soil
412 with the high K_s–value, only RIA ran to completion. The discontinuity of the first derivative
413 at the air-entry value did not cause numerical problems. In fact, the replacement of any
414 parametric expression by a look-up table creates a discontinuity of the first derivative at
415 every point of the look-up table.

416 Table 4 lists the main mean annual fluxes calculated from the simulation study. The
417 median flux was produced by RIA for all combinations of soil and climate. The mean annual
418 actual transpiration between the three parameterizations differed by more than 10% from
419 the median only for the silt loam under a temperate climate. The actual evaporation only
420 deviated more than 10% for the loamy sand under a semi-arid climate. The amount of
421 water leaving the soil profile differed substantially between parameterizations for the semi-
422 arid and temperate climate, especially for VGA (20–46% deviation from the median).

423 The daily data revealed significant differences on smaller time scales that will be
424 relevant if reactive solute transport is of interest (see the Supplement). The fluxes
425 generated by the VGA parameterizations responded more quickly and strongly to the
426 rainfall signal, with VGN and RIA giving a more delayed and smooth response. The SWRCs
427 (Fig. 1) offer no explanation for this, but Fig. 2 shows that VGA's hydraulic conductivity in
428 the wet and intermediate water content range for all three soils is considerably higher than
429 that of VGN and RIA, except for clay, where it is only moderately higher than RIA's and
430 drops below RIA at a water content of 0.28. Thus, small differences between SWRCs can
431 have a significant influence on soil water flow simulations through the effect of their

parameters on the soil hydraulic conductivity curve, an effect that the reviews by Leij et al. (1997) and Assouline and Or (2013) took into consideration to some degree, but was not considered in several other studies that compared different parameterizations (e.g., Rossi and Nimmo, 1994; Assouline et al., 1998; Cornelis et al., 2005; Khlosi et al., 2008).

436 Table 4. Average of the annual sums of the actual transpiration and evaporation, and of the
437 outflow across the lower boundary of the simulated soil profiles. The averages were
438 calculated for the final six years of the simulation periods. The values in parentheses are
439 scaled with respect to the corresponding value for RIA.

Climate	Soil	Actual transpiration (mm)			Actual evaporation (mm)			Downward flux at 2 m depth (mm)		
		RIA	VGA	VGN	RIA	VGA	VGN	RIA	VGA	VGN
Monsoon	clay	962	–	–	543	–	–	876	–	–
	silt loam	1114	1044 (0.94)	1112 (1.06)	541	554 (1.02)	534 (0.96)	711	763 (1.07)	718 (0.94)
	loamy sand	1037	976 (0.94)	1024 (1.05)	480	440 (0.92)	461 (1.05)	863	959 (1.11)	896 (0.93)
Semi–arid	clay	585	–	–	319	–	–	294	–	–
	silt loam	657	588 (0.90)	653 (1.11)	297	303 (1.02)	287 (0.95)	164	226 (1.37)	177 (0.78)
	loamy sand	585	540 (0.92)	572 (1.06)	248	222 (0.89)	234 (1.06)	290	363 (1.25)	319 (0.88)
Temperate	clay	202	–	–	163	–	–	167	–	–
	silt loam	281	236 (0.84)	271 (1.15)	150	151 (1.01)	143 (0.95)	99	144 (1.46)	114 (0.79)
	loamy sand	224	205 (0.92)	214 (1.04)	130	118 (0.91)	124 (1.05)	174	208 (1.20)	190 (0.91)

440

Summary and Conclusions

The improvements incorporated in the RIA parameterization for the first time remove problems of the popular VGN model in both the wet and the dry range while retaining the desirable sigmoid shape in the mid–range. This shape allows its multimodal version to represent SWRCs with multiple humps. RIA offers a wider range of shapes for the conductivity curve than any other parameterization that does not lead to the unphysical behavior near saturation that was revealed by Durner (1994) and Ippisch et al. (2006) for VGN and by Madi et al. (2018) for 14 other parameterizations. RIA also proved to be more robust during numerical simulations than VGN itself as well as its modification VGA, which still has a non–physical asymptote at a non–zero residual water content. The deep drainage generated by RIA was more spread out and smaller than the spiked response to rainfall produced by VGA, probably because RIA was better able to produce a conductivity curve with a substantial drop during the early stages of drying. We therefore hope that RIA or its multimodal version will be adopted for use in numerical simulations of soil water flow. The catalogue of parameters for 21 soils in Appendix C may be of help for such simulations.

Appendix A. List of Abbreviations

BC: Brooks and Corey (1964)

BCO: parameterization of the SWRC according to the original Brooks and Corey (1964) equation

FSB: parameterization of the SWRC according to the BC–based version of Fayers and Simmons (1995)

RIA: parameterization of the SWRC that combines RNA and VGA

RNA: parameterization of the SWRC according to the junction model of Rossi and Nimmo (1994)

SWRC: soil water retention curve

RMSE: root mean square error

UNSODA: unsaturated soil hydraulic properties database

VGA: parameterization of the SWRC according to Ippisch et al. (2016)

VGN: parameterization of the SWRC according to the original van Genuchten (1980) equation

Appendix B. Assessing the near-saturation behavior of recently developed soil water retention and hydraulic conductivity curves

Madi et al. (2018) developed a criterion that needs to be met to avoid unphysical behavior of the unsaturated soil hydraulic conductivity curve near saturation:

$$\lim_{h\uparrow 0}\left(|h|^{-\kappa}\frac{\mathrm{d}\theta}{\mathrm{d}h}\right)=0 \tag{B1}$$

where κ is a fitting parameter (>0) that appears in a several parameterizations of the unsaturated soil hydraulic conductivity curve based on the capillary bundle conceptualization.

Fredlund and Xing (1994) introduced the following parameterization for the soil water retention curve:

$$\theta(h)=\left[\frac{-\ln\left(1+\frac{|h|}{|h_\mathrm{r}|}\right)}{\ln\left(1+\frac{b}{|h_\mathrm{r}|}\right)}+1\right]\frac{\theta_\mathrm{s}}{\left\{\ln\left[\mathrm{e}+\left(\frac{|h|}{a}\right)^{n}\right]\right\}^{m}} \tag{B2}$$

where the subscript 'r' denotes the value when the residual water content is reached, and a [L], n, and m are fitting parameters. The first term on the right-hand side is a correction term that forces the water content to zero for $h=-b$, with b equal to 10^7 cm (Fredlund and Xing, 1994) or 6.3×10^6 cm (Wang et al., 2016). Wang et al. (2016) also modified the correction factor to give

$$\theta(h) = \left[\frac{-\ln\left(1+\frac{c|h|}{|h_r|}\right)}{\ln\left(1+\frac{bc}{|h_r|}\right)} + 1\right]\frac{\theta_s}{\left\{\ln\left[e+\left(\frac{|h|}{a}\right)^n\right]\right\}^m} \quad \text{(B3)}$$

where c has to be small and positive. The derivative of Eq. (B3) is

$$\frac{d\theta}{dh} = \frac{-\theta_s}{\left\{\ln\left[e+\left(\frac{|h|}{a}\right)^n\right]\right\}^m}\left\{\frac{mn|h|^{n-1}\left[\ln\left(1+\frac{bc}{|h_r|}\right)\ln\left(1+\frac{c|h|}{|h_r|}\right)-1\right]}{a^n\left[e+\left(\frac{|h|}{a}\right)^n\right]\ln\left[e+\left(\frac{|h|}{a}\right)^n\right]} - \frac{\ln\left(1+\frac{bc}{|h_r|}\right)}{\frac{|h_r|}{c}+|h|}\right\} \quad \text{(B4)}$$

The derivative of Eq. (B2) follows by setting c equal to 1 in Eq. (B4). Combining Eq.(B4) with Eq. (B1) results in the following requirement:

$$\lim_{h\uparrow 0}\left[\frac{\theta_s mn}{ea^n}|h|^{-\kappa+n-1} + \frac{c\theta_s\ln\left(1+\frac{bc}{|h_r|}\right)}{|h_r|}|h|^{-\kappa}\right]=0 \quad \text{(B5)}$$

The limit goes to zero if and only if the exponents in both terms are positive. Hence, $\kappa < n-1$ and $\kappa < 0$. The first requirement may be met for some soils, but the second violates the physical constraint that κ cannot be negative (Madi et al., 2018). Therefore, neither Fredlund and Xing's (1994) nor Wang et al.'s (2016) parameterization lead to unsaturated hydraulic conductivity curves that exhibit physically realistic behavior near saturation. Wang et al. (2018) added a modification in the dry end of Wang et al. (2016), and Rudiyanto et al. (2020) in turn used Wang et al.'s (2018) curves. Because the problem near saturation was not resolved, these two hydraulic conductivity models suffer from the same problem near saturation.

Appendix C. Fitted Parameters and Root Mean Square Error for Six Parameterizations of the Soil Water Retention Curve applied to Data of 21 Soils

The UNSODA soils selected for parameter fitting are grouped in Tables C1–C4 according to their texture classification according to Twarakavi et al. (2010). Sand is a major constituent of the mineral soil in Tables C1 and C2, silt in Table C3, and clay in Table C4. Figure C1 shows the textural composition of the soils. For each soil, the parameter values for six parameterizations are given, resulting in a total of 126 SWRC parameterizations. The Root Mean Square Errors (RMSE) for all fits are listed in Tables C5–C8. The saturated hydraulic conductivities of the soils as given by the UNSODA database are given in Table C9.

Madi et al. (2018) provide an analysis of the underlying functions of all parameterizations tested here, except RIA. The meaning of all variables except λ is explained in the main text. Variable λ is the power to which the factor (h / h_{ae}) is raised in the power–law segments of the SWRCs of BCO, FSB, and RNA. In RNA, λ is expressed as a function of the fitting parameters, and therefore does not appear in the tables.

The SWRCs defined by these parameterizations together with the data points on which they are based are given in Figs. C2–C5. The hydraulic conductivity curves according to Mualem (1976) that can be derived from the parameterizations (Eqs. (13a) and (13b) for RIA, equations for the other parameterizations in Madi et al. (2018)) are plotted in Figs. C6–C9. We plotted K as a function of θ because this relationship is less hysteretic than $K(h)$

(Koorevaar et al., 1983, p. 141) and some of the UNSODA data only provided $K(\theta)$ data points. The conductivity data available in UNSODA are also plotted, but these were not used to fit the curves to. The maximum pF value for which points on the curves were calculated was set at 6.8 for VGN and VGA, and to the pF value corresponding to the fitted value of h_d for RIA.

The comparison of theoretical conductivity curves based on water retention data with the measured values showed a sometimes substantial deviation between hydraulic conductivities measured at saturation and the K_s value used to create the theoretical curves. The latter value was obtained by a query that made the database return a K_s value for the soils that met all other criteria also included in the query. The conductivity data displayed in the plots were separately obtained by requesting the database to return a report of tabular data for each of the 21 soils. The reasons for the discrepancies between the queried value and the tabulated may reflect separate experiments for measuring unsaturated and saturated values of K.

There also are obvious differences between the water content at saturation between the retention and the conductivity data. In all but one case (soil 4450, Fig. C8) the hydraulic conductivity observations were made in the field whereas the retention data used were all obtained from drying experiments in the laboratory. Scale differences, effects of air enclosure and hysteresis in the field, and differences between different measurement techniques explain these differences. We can therefore only compare the shape of the theoretical curves with those of the data clouds.

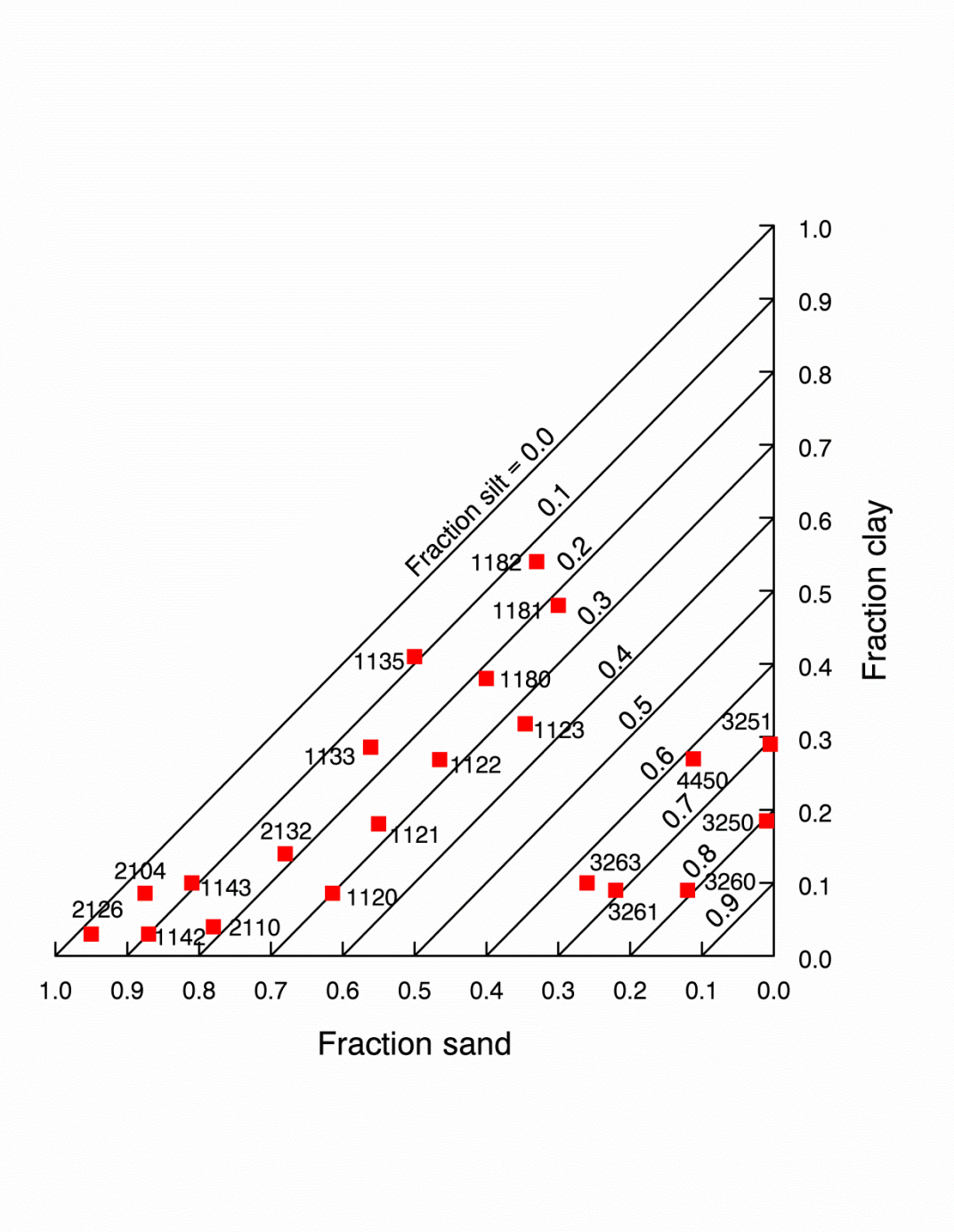

558

559 Figure C1. The positions in the texture triangle of the selected soils, indicated by their

560 UNSODA identifier. (Taken form Madi et al., 2018)

561

562 The RMSE was calculated from the weighted sum of squares of the differences
563 between calculated and observed water contents and pressure heads. The weights equaled
564 the estimated scaled standard deviations of the individual water retention observations
565 (pairs of matric potential and water content values). The standard deviations of the water
566 content observations were scaled to have an average value of 0.2. The scale factor needed to
567 arrive at this value was then applied to the standard deviations of the matric potential
568 values as well. This ensured that the weighting of water contents and matric potential
569 values was consistent with the original standard deviations of both. The scaling greatly
570 improved the efficiency of the parameter fitting procedure. The squared difference between
571 a single observed water content and its fitted value during a given iteration of the
572 parameter fitting algorithm, taking into account observation errors in both the water
573 content and the matric potential, is
574
575 $$\left(\frac{\theta_{\mathrm{fit}}-\theta_{\mathrm{obs}}}{\sigma_{\theta,\,\mathrm{scaled}}+\sigma_{h,\mathrm{scaled}}\frac{d\theta}{dh}\Big|_{h_{\mathrm{obs}}}}\right)^2 \qquad \text{(C1)}$$
576
577 where $\sigma_{a,\,\mathrm{scaled}}$ is the scaled standard deviation of the variable *a*, subscript 'fit' signifies a
578 fitted value of the subscripted variable, and subscript 'obs' a measured value (Madi et al.,
579 2018). The slope of the SWRC in the denominator is estimated from the fitted
580 parameterization using the parameter values that have been fitted in the iteration that is
581 currently being tested.
582 The scale factors applied to the observation error standard deviations varied
583 between soils but not between parameterizations fitted to the same soil. RMSE values of

584 different parameterizations valid for a particular soil can therefore be readily compared.
585 Comparisons between soils only give a rough indication. When the water contents at which
586 measurements were taken differ strongly from one soil to another, the comparison of their
587 RMSE values is less reliable.

588 In case the measured water contents were obtained at hydrostatic equilibrium, the
589 fitted water content calculated directly from the matric potential could not be compared to
590 the observed water content. To approximate the soil sample on which the observation was
591 made, a hypothetical soil slab of the same height as the sample was divided into 20
592 horizontal layers. If UNSODA did not specify the sample height, it was assumed to be 5.0 cm.
593 The matric potential in the center of each layer was determined from the given matric
594 potential, which was assumed to apply to the center of the sample. The water content of the
595 soil slab was then calculated as the average water content of its 20 layers. This water
596 content was used to calculate the difference between the observed and the fitted water
597 content. Figure C10 shows a comparison of retention points calculated for three soils based
598 directly on the RIA parameterization and based on the same parameterization applied to a
599 hypothetical sample of 5.0 cm height at hydrostatic equilibrium with the nominal matric
600 potential valid at the sample center. Deviations are small, even for the loamy sand.

Table C1. The fitting parameters and their values for six parameterizations for sandy soils in the A1 and A2 classifications of Twarakavi et al. (2010) from the UNSODA database (National Agricultural Library, 2017; Nemes et al., 2001). The three–character parameterization label is explained in the main text.

			Soil (UNSODA identifier and classification according to Twarakavi et al. (2010))		
			2126 A1	1142 A2	2104 A2
Parameter–ization	Parame–ter	Unit			
BCO	θ_r	–	1.63E–2	4.92E–5	2.27E–2
	θ_s	–	0.377	0.250	0.398
	h_{ae}	cm	–6.78	–7.00	–6.79
	λ	–	0.846	0.210	0.434
FSB	θ_s	–	0.377	0.250	0.398
	θ_a	–	2.58E–2	6.26E–5	5.46E–2
	h_{ae}	cm	–6.76	–7.00	–6.73
	λ	–	0.861	0.211	0.468
RNA	θ_s	–	0.378	0.250	0.398
	h_{ae}	cm	–6.37	–7.00	–6.17
	h_j	cm	–8.87E4	–9.24E4	–6.45E4
	h_d	cm	–3.60E5	–1.07E7	–9.73E5
VGN	θ_r	–	3.39E–2	9.42E–2	3.41E–2
	θ_s	–	0.376	0.242	0.398
	α	cm^{-1}	6.85E–2	1.99E–2	6.97E–2
	n	–	2.73	2.93	1.64
VGA	θ_r	–	3.39E–2	9.64E–2	3.42E–2
	θ_s	–	0.376	0.242	0.398
	α	cm^{-1}	6.84E–2	1.98E–2	6.97E–2
	n	–	2.73	3.05	1.64
	h_{ae}	cm	–0.101	–0.240	–1.62E–2
RIA	θ_s	–	0.378	0.245	0.398
	α	cm^{-1}	0.239	2.68E–2	0.171
	n	–	1.77	1.47	1.41
	h_{ae}	cm	–5.82	–7.00	–4.36
	h_j	cm	–1.76E6	–4.35E5	–7.75E5

606 Table C2. The fitting parameters and their values for six parameterizations for sandy soils in the A3
607 and A4 classifications of Twarakavi et al. (2010) from the UNSODA database (National Agricultural
608 Library, 2017; Nemes et al., 2001). The three–character parameterization label is explained in the
609 main text.

			Soil (UNSODA identifier and classification according to Twarakavi et al. (2010))					
			1120 A3	1143 A3	2110 A3	2132 A3	1121 A4	1133 A4
Para–meteri–zation	Para me–eter	Unit						
BCO	θ_r	–	6.15E–6	2.71E–5	0.103	4.10E–5	2.64E–5	5.37E–5
	θ_s	–	0.311	0.279	0.348	0.303	0.350	0.330
	h_{ae}	cm	–10.0	–7.00	–25.5	–8.00	–10.0	–206
	λ	–	0.204	0.169	0.537	0.107	0.118	0.103
FSB	θ_s	–	0.311	0.279	0.348	0.308	0.346	0.330
	θ_a	–	4.33E–5	4.26E–4	0.213	0.298	0.324	0.310
	h_{ae}	cm	–10.0	–7.00	–25.7	–3.24	–10.0	–206
	λ	–	0.204	0.169	0.763	0.422	0.377	0.213
RNA	θ_s	–	0.311	0.279	0.351	0.303	0.352	0.330
	h_{ae}	cm	–10.0	–7.00	–20.3	–8.00	–10.0	–220
	h_j	cm	–7.32E4	–8.46E4	–6.44E4	–7.18E4	–8.73E4	–6.77E4
	h_d	cm	–9.95E6	–3.18E7	–2.35E6	–8.06E8	–3.88E8	–8.68E8
VGN	θ_r	–	7.22E–2	9.24E–2	0.126	1.25E–4	1.70E–5	0.202
	θ_s	–	0.305	0.278	0.360	0.305	0.339	0.324
	α	cm^{-1}	1.72E–2	4.66E–2	2.63E–2	5.73E–2	7.21E–3	7.34E–4
	n	–	1.69	1.49	1.84	1.14	1.26	3.02
VGA	θ_r	–	7.37E–2	0.112	0.106	6.61E–4	1.47E–5	0.202
	θ_s	–	0.303	0.276	0.348	0.306	0.339	0.324
	α	cm^{-1}	1.72E–2	4.41E–2	0.230	6.06E–2	7.16E–3	7.35E–4
	n	–	1.71	1.66	1.56	1.14	1.27	3.00
	h_{ae}	cm	–9.37	–6.81	–25.3	–8.47E–4	–2.73E–2	–12.5
RIA	θ_s	–	0.308	0.280	0.360	0.306	0.339	0.328
	α	cm^{-1}	3.01E–2	6.39E–2	4.18E–2	6.08E–2	7.13E–2	1.30E–3
	n	–	1.29	1.23	1.33	1.14	1.27	1.20
	h_{ae}	cm	–1.24E–3	–4.96E–4	–7.85	–7.44E–4	–9.11E–4	–220
	h_j	cm	–1.71E6	–7.01E6	–9.37E6	–7.81E6	–2.04E6	–5.07E6

Table C3. The fitting parameters and their values for six parameterizations for silty soils from the UNSODA database (National Agricultural Library, 2017; Nemes et al., 2001). The three–character parameterization label is explained in the main text.

			Soil (UNSODA identifier and classification according to Twarakavi et al. (2010))					
			3260 B2	3261 B2	3263 B2	3250 B4	3251 B4	4450 B4
Para–meteri–zation	Para me–ter	Unit						
BCO	θ_r	–	2.85E–6	3.42E–6	3.85E–7	3.85E–6	1.94E–6	2.77E–5
	θ_s	–	0.470	0.499	0.460	0.540	0.500	0.380
	h_{ae}	cm	–28.6	–13.5	–28.8	–30.5	–18.2	–4.80
	λ	–	0.281	0.256	0.255	0.183	9.56E–2	9.51E–2
FSB	θ_s	–	0.470	0.499	0.460	0.540	0.500	0.380
	θ_a	–	1.33E–5	6.49E–5	1.33E–5	0.173	0.431	0.320
	h_{ae}	cm	–28.6	–13.5	–28.8	–30.0	–10.9	–0.882
	λ	–	0.281	0.256	0.255	0.241	0.197	0.196
RNA	θ_s	–	0.470	0.499	0.460	0.540	0.500	0.380
	h_{ae}	cm	–28.6	–13.5	–28.8	–30.5	–18.2	–4.81
	h_j	cm	–9.23E4	–9.43E4	–7.48E4	–7.87E4	–1.97E4	–2.63E4
	h_d	cm	–3.23E6	–4.96E6	–3.75E6	–6.86E6	–7.66E8	–9.69E8
VGN	θ_r	–	5.25E–2	4.88E–2	4.48E–2	3.10E–2	1.60E–5	1.16E–6
	θ_s	–	0.472	0.491	0.461	0.540	0.501	0.379
	α	cm^{-1}	1.62E–2	1.84E–2	1.53E–2	1.21E–2	2.62E–2	0.164
	n	–	1.47	1.51	1.41	1.28	1.11	1.10
VGA	θ_r	–	5.27E–2	4.89E–2	6.12E–2	3.80E–4	7.21E–5	2.80E–5
	θ_s	–	0.472	0.491	0.457	0.540	0.500	0.379
	α	cm^{-1}	1.62E–2	1.84E–2	1.49E–2	1.33E–2	3.66E–2	1.26
	n	–	1.47	1.52	1.46	1.25	1.11	1.10
	h_{ae}	cm	–3.26E–3	–2.08E–3	–15.1	–4.87	–7.31	–4.54
RIA	θ_s	–	0.474	0.493	0.463	0.540	0.500	0.379
	α	cm^{-1}	2.04E–2	2.33E–2	1.86E–2	1.33E–2	3.57E–2	0.164
	n	–	1.33	1.37	1.31	1.25	1.11	1.10
	h_{ae}	cm	–5.95E–3	–2.36E–3	–2.43E–3	–4.80	–7.12	–1.21E–3
	h_j	cm	–1.49E6	–1.07E6	–8.62E6	–8.02E6	–8.33E6	–9.89E6

Table C4. The fitting parameters and their values for six parameterizations for clayey soils from the UNSODA database (National Agricultural Library, 2017; Nemes et al., 2001). The three–character parameterization label is explained in the main text.

			Soil (UNSODA identifier and classification according to Twarakavi et al. (2010))					
			1135 C2	1182 C2	1122 C4	1123 C4	1180 C4	1181 C4
Para–meteri–zation	Para–meter	Unit						
BCO	θ_r	–	3.94E–4	1.79E–4	2.64E–4	2.13E–4	5.22E–4	1.24E–5
	θ_s	–	0.420	0.549	0.362	0.358	0.497	0.456
	h_{ae}	cm	–106	–0.977	–10.0	–10.0	–11.1	–5.17
	λ	–	7.85E–2	4.41E–2	3.37E–2	2.69E–2	5.65E–2	5.40E–2
FSB	θ_s	–	0.420	0.548	0.360	0.356	0.495	0.456
	θ_a	–	0.400	0.307	0.350	0.340	0.491	0.345
	h_{ae}	cm	–106	–0.230	–5.75	–10.0	–8.58	–13.2
	λ	–	0.172	5.64E–2	6.60E–2	5.69E–2	100	8.08E–2
RNA	θ_s	–	0.420	0.549	0.370	0.370	0.497	0.456
	h_{ae}	cm	–106	–3.61	–9.99	–9.99	–0.150	–7.66
	h_j	cm	–107	–12.2	–10.5	–10.7	–24.1	–22.1
	h_d	cm	–1.64E8	–1.00E9	–1.00E9	–1.00E9	–1.00E9	–1.00E9
VGN	θ_r	–	0.263	8.94E–6	1.16E–4	0.210	0.255	3.34E–6
	θ_s	–	0.413	0.548	0.359	0.354	0.496	0.456
	α	cm^{-1}	1.02E–3	0.753	1.37E–2	2.92E–3	0.805	0.143
	n	–	2.37	1.05	1.05	1.21	1.26	1.06
VGA	θ_r	–	0.263	1.19E–5	5.78E–2	0.188	2.63E–2	2.12E–6
	θ_s	–	0.413	0.548	0.359	0.354	0.498	0.456
	α	cm^{-1}	1.02E–3	1.21	1.37E–2	3.22E–3	10.1	1.70
	n	–	2.37	1.05	1.07	1.17	1.06	1.05
	h_{ae}	cm	–1.03	–0.467	–4.18E–2	–10.0	–1.11E–2	–4.83
RIA	θ_s	–	0.416	0.548	0.359	0.354	0.497	0.457
	α	cm^{-1}	1.86E–3	1.31	1.39E–2	4.00E–3	14.2	0.702
	n	–	1.16	1.05	1.05	1.06	1.06	1.05
	h_{ae}	cm	–106	–0.525	–3.80E–3	–9.99	–4.41E–2	–4.25
	h_j	cm	–7.57E6	–9.97E6	–9.56E4	–4.43E6	–415	–206

618 Table C5. Root mean square errors of the parameter fits for the sandy or loamy soils (A1 and A2
619 soils according to Twarakavi et al., 2010)

	Soil (UNSODA identifier and classification according to Twarakavi et al. (2010))		
Parameterization	2126 A1	1142 A2	2104 A2
BCO	0.0620	0.0990	0.0481
FSB	0.0626	0.0990	0.0517
RNA	0.0659	0.0989	0.0553
VGN	0.0330	0.0252	0.0278
VGA	0.0330	0.0250	0.0278
RIA	0.0652	0.0504	0.0542

620

621

622 Table C6. Root mean square errors of the parameter fits for the sandy soils (A3 and A4 soils
623 according to Twarakavi et al., 2010)

Parameterization	Soil (UNSODA identifier and classification according to Twarakavi et al. (2010))					
	1120 A3	1143 A3	2110 A3	2132 A3	1121 A4	1133 A4
BCO	0.0926	0.0501	0.0445	0.0356	0.1288	0.0803
FSB	0.0926	0.0500	0.0445	0.0292	0.1054	0.0700
RNA	0.0926	0.0500	0.0457	0.0356	0.1286	0.0775
VGN	0.0446	0.0333	0.0378	0.0204	0.0720	0.0175
VGA	0.0489	0.0396	0.0445	0.0203	0.0720	0.0175
RIA	0.0643	0.0346	0.0491	0.0203	0.0720	0.0530

624

625

626 Table C7. Root mean square errors of the parameter fits for the silty soils.

Parameterization	Soil (UNSODA identifier and classification according to Twarakavi et al. (2010))					
	3260 B2	3261 B2	3263 B2	3250 B4	3251 B4	4450 B4
BCO	0.0793	0.1316	0.0973	0.0822	0.0551	0.0499
FSB	0.0794	0.1316	0.0973	0.0815	0.0395	0.0445
RNA	0.0793	0.1316	0.0973	0.0822	0.0551	0.0499
VGN	0.0456	0.0607	0.0638	0.0413	0.0474	0.0485
VGA	0.0455	0.0607	0.0769	0.0412	0.0466	0.0497
RIA	0.0543	0.0698	0.0668	0.0412	0.0466	0.0485

627

628

629 Table C8. Root mean square errors of the parameter fits for the clayey soils.

Parameterization	Soil (UNSODA identifier and classification according to Twarakavi et al. (2010))					
	1135 C2	1182 C2	1122 C4	1123 C4	1180 C4	1181 C4
BCO	0.0913	0.0494	0.0349	0.0489	0.0187	0.0428
FSB	0.0721	0.0441	0.0212	0.0321	0.1196	0.0360
RNA	0.0812	0.0913	0.1235	0.1501	0.0347	0.0570
VGN	0.0208	0.0488	0.0197	0.0244	0.0411	0.0433
VGA	0.0208	0.0485	0.0198	0.0243	0.0197	0.0429
RIA	0.0519	0.0485	0.0197	0.0244	0.0180	0.0391

630

631

632 Table C9. Values for the hydraulic conductivity at saturation (K_s) for the selected soils from
633 the UNSODA database. The soils are identified by their UNSODA identifier. Their classification
634 according to Twarakavi et al. (2010) is also given.

UNSODA identifier	Texture classification	K_s (cm d^{-1})
2126	A1	1.10E3
1142	A2	13.4
2104	A2	553
1120	A3	37.9
1143	A3	23.5
2110	A3	16.3
2132	A3	5.52
1121	A4	7.13
1133	A4	7.13
3260	B2	10.8
3261	B2	32.0
3263	B2	54.0
3250	B4	1.51
3251	B4	2.74
4450	B4	1.20
1135	C2	0.142
1182	C2	1.25
1122	C4	2.92
1123	C4	0.740
1180	C4	215
1181	C4	178

635

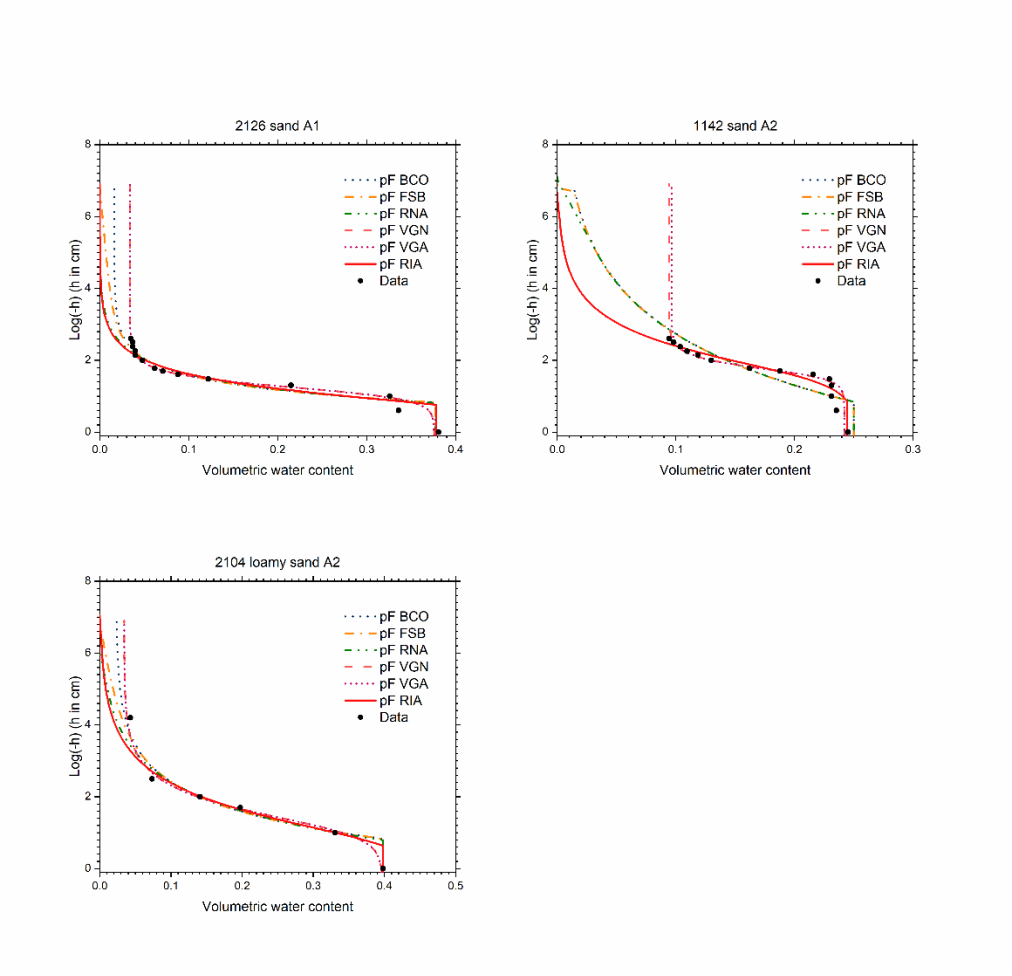

636

637 Figure C2. Retention data and fitted soil water retention curves according to six

638 parameterizations for selected UNSODA soils with Twarakavi et al.'s (2010) A1 or A2

639 classification. The parameterizations are explained in the text.

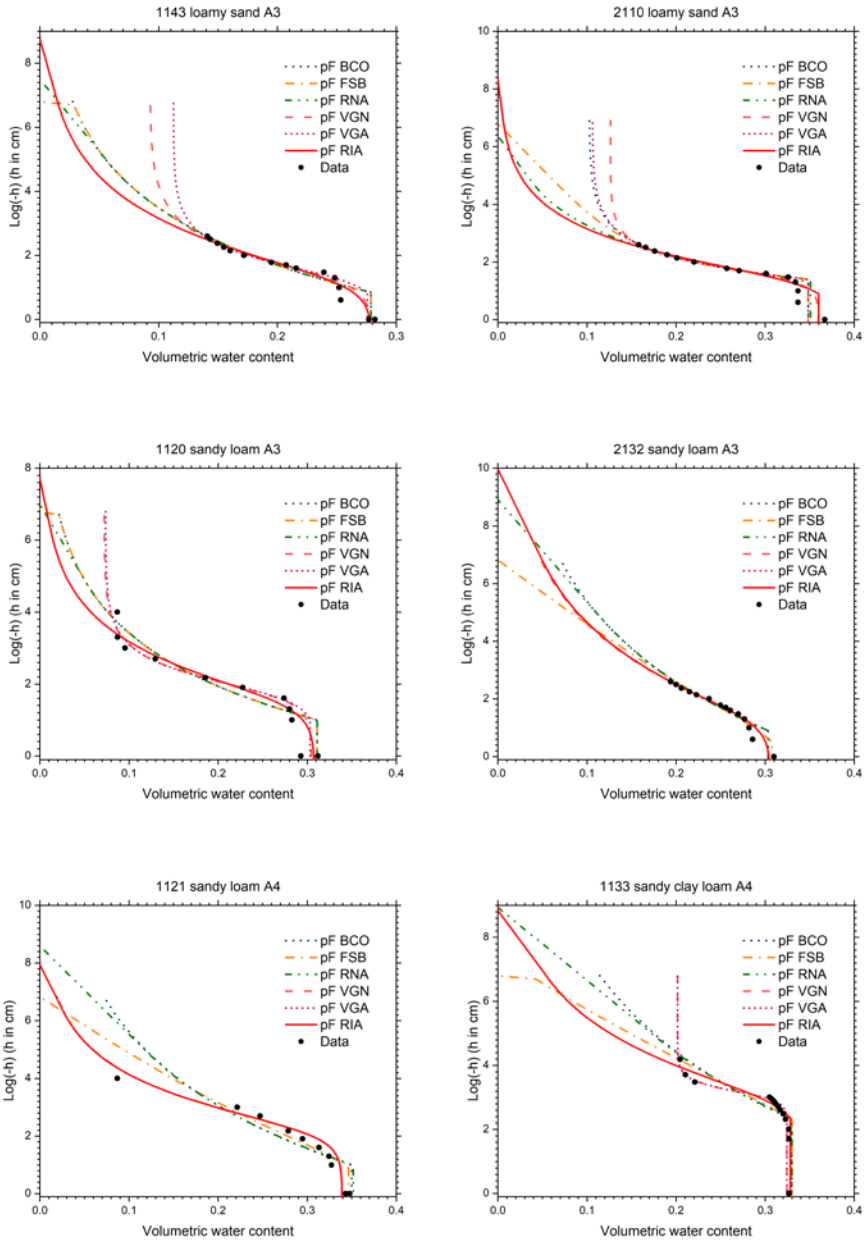

640

641 Figure C3. Retention data and fitted soil water retention curves according to six

642 parameterizations for selected UNSODA soils with Twarakavi et al.'s (2010) A3 or A4

643 classification. The parameterizations are explained in the text.

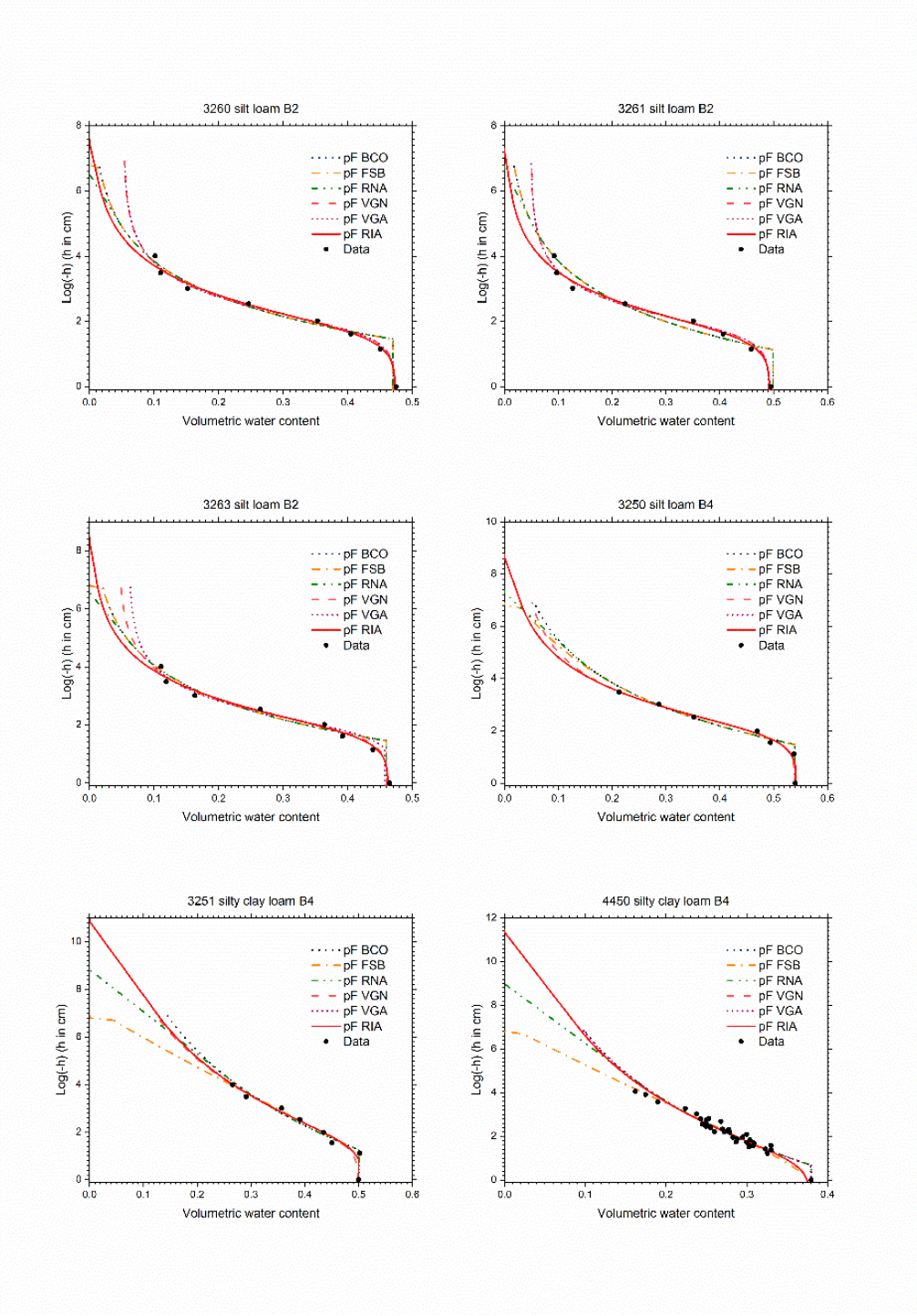

644

645 Figure C4. Retention data and fitted soil water retention curves according to six

646 parameterizations for selected UNSODA soils with Twarakavi et al.'s (2010) B2 or B4

647 classification. The parameterizations are explained in the text.

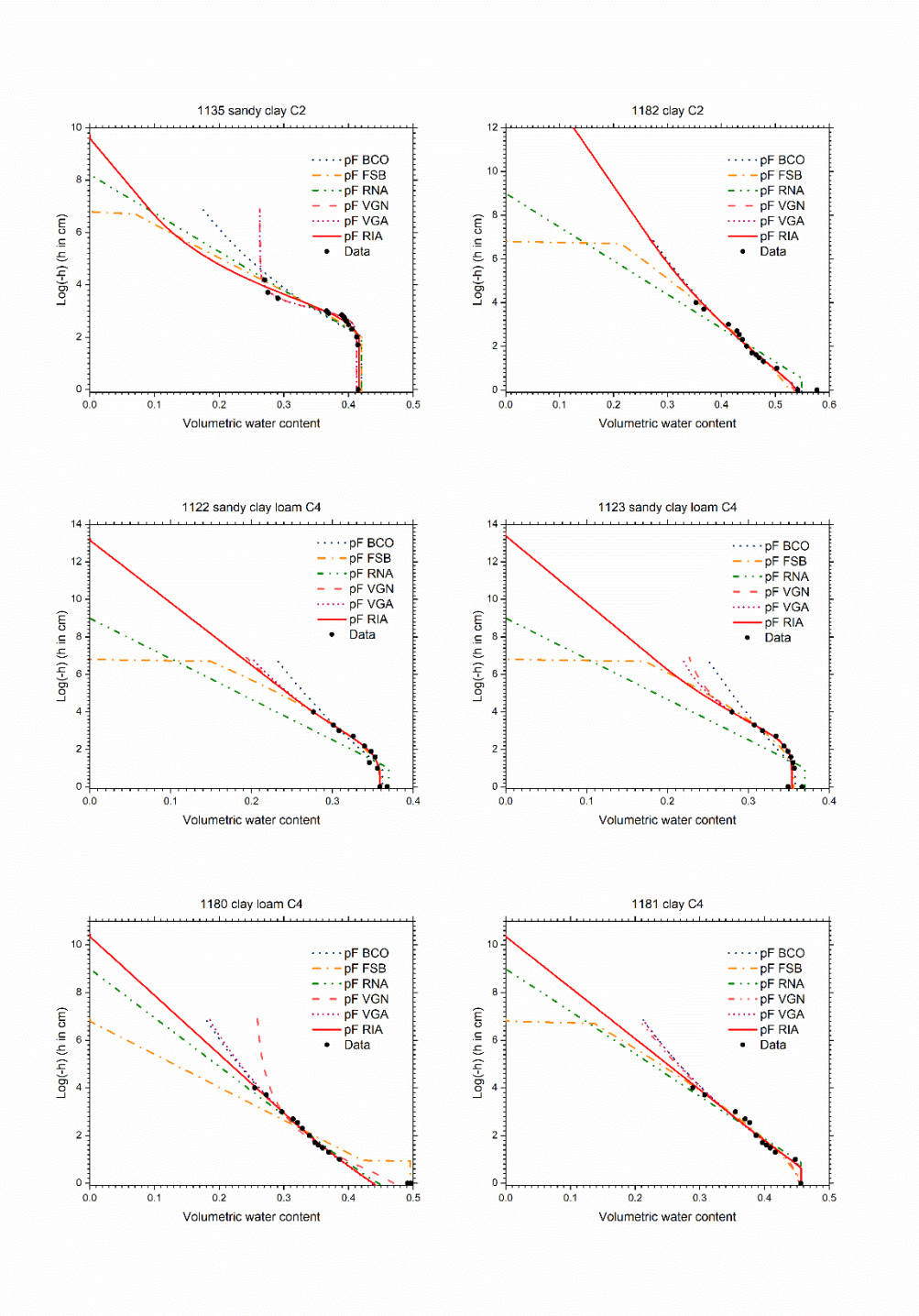

Figure C5. Retention data and fitted soil water retention curves according to six parameterizations for selected UNSODA soils with Twarakavi et al.'s (2010) C2 or C4 classification. The parameterizations are explained in the text.

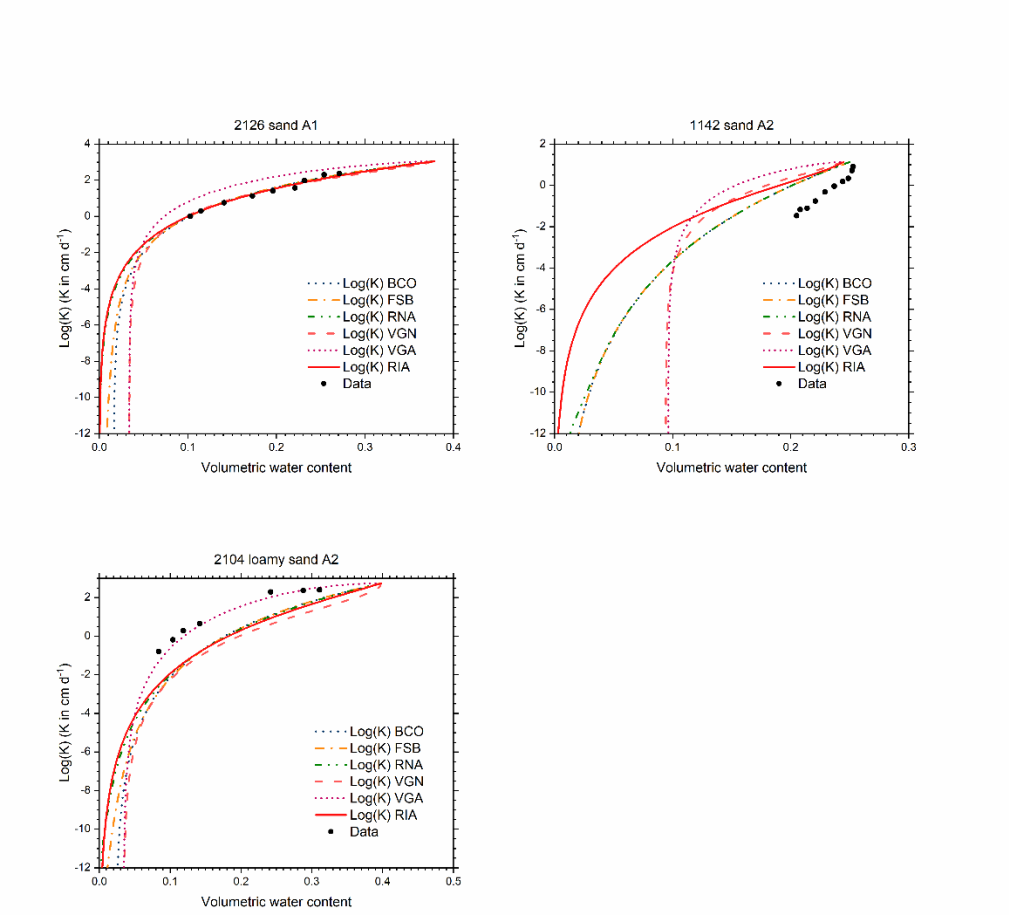

652

653 Figure C6. Conductivity data and conductivity curves derived from the retention curves of

654 Fig. C2 according to six parameterizations for selected UNSODA soils with Twarakavi et al.'s

655 (2010) A1 or A2 classification.

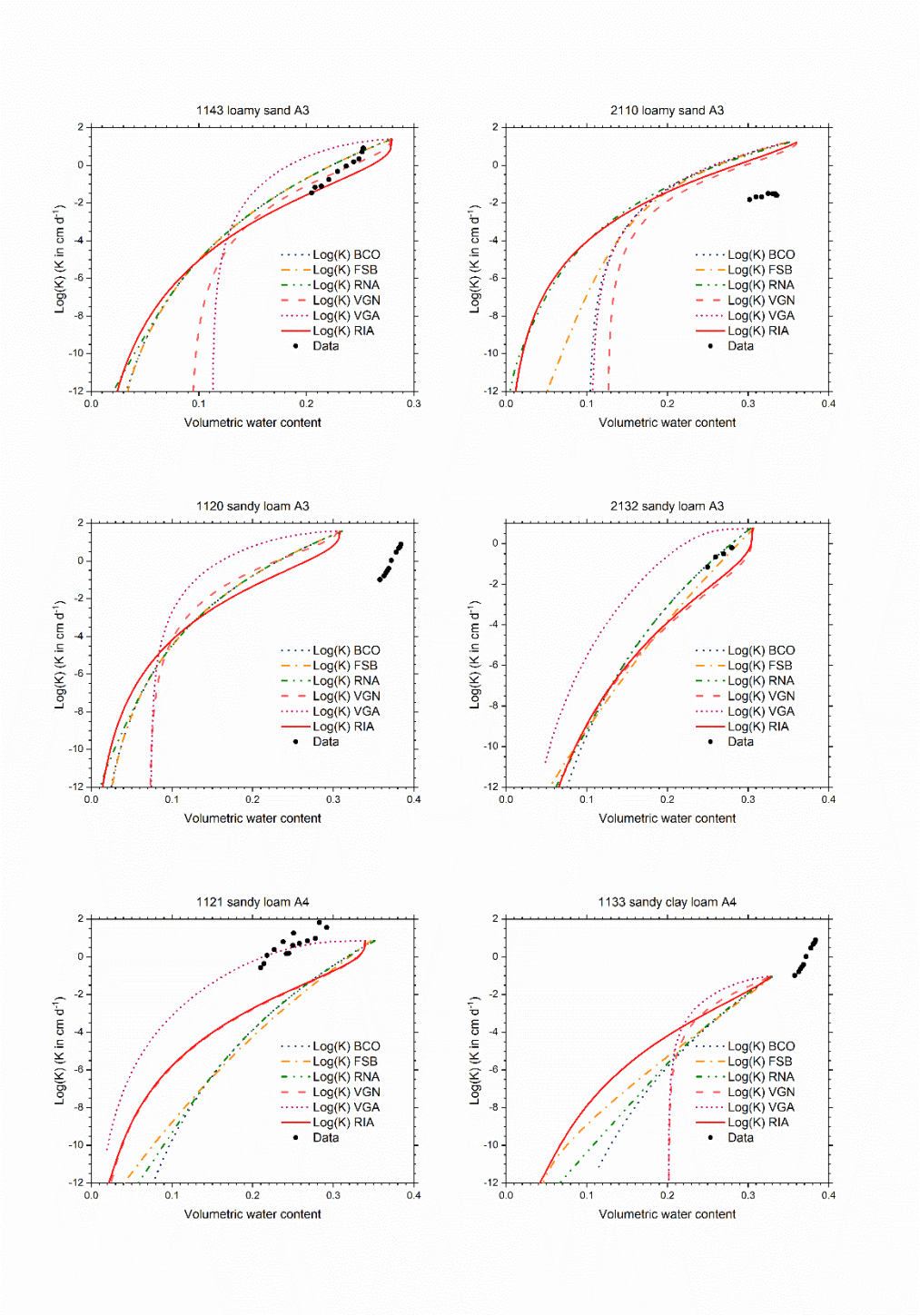

Figure C7. Conductivity data and conductivity curves derived from the retention curves of Fig. C3 according to six parameterizations for selected UNSODA soils with Twarakavi et al.'s (2010) A3 or A4 classification.

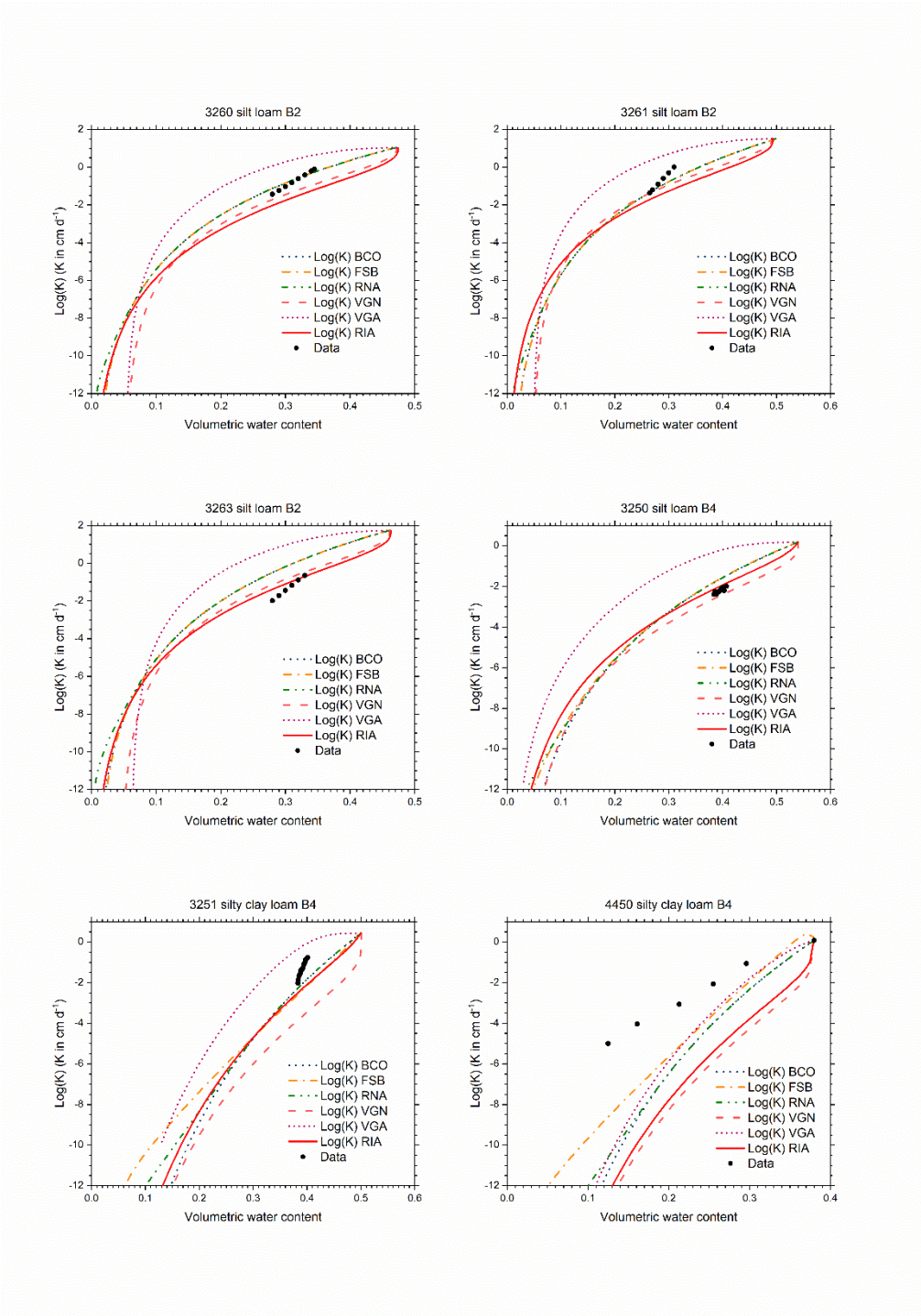

660

661 Figure C8. Conductivity data and conductivity curves derived from the retention curves of

662 Fig. C4 according to six parameterizations for selected UNSODA soils with Twarakavi et al.'s

663 (2010) B2 or B4 classification.

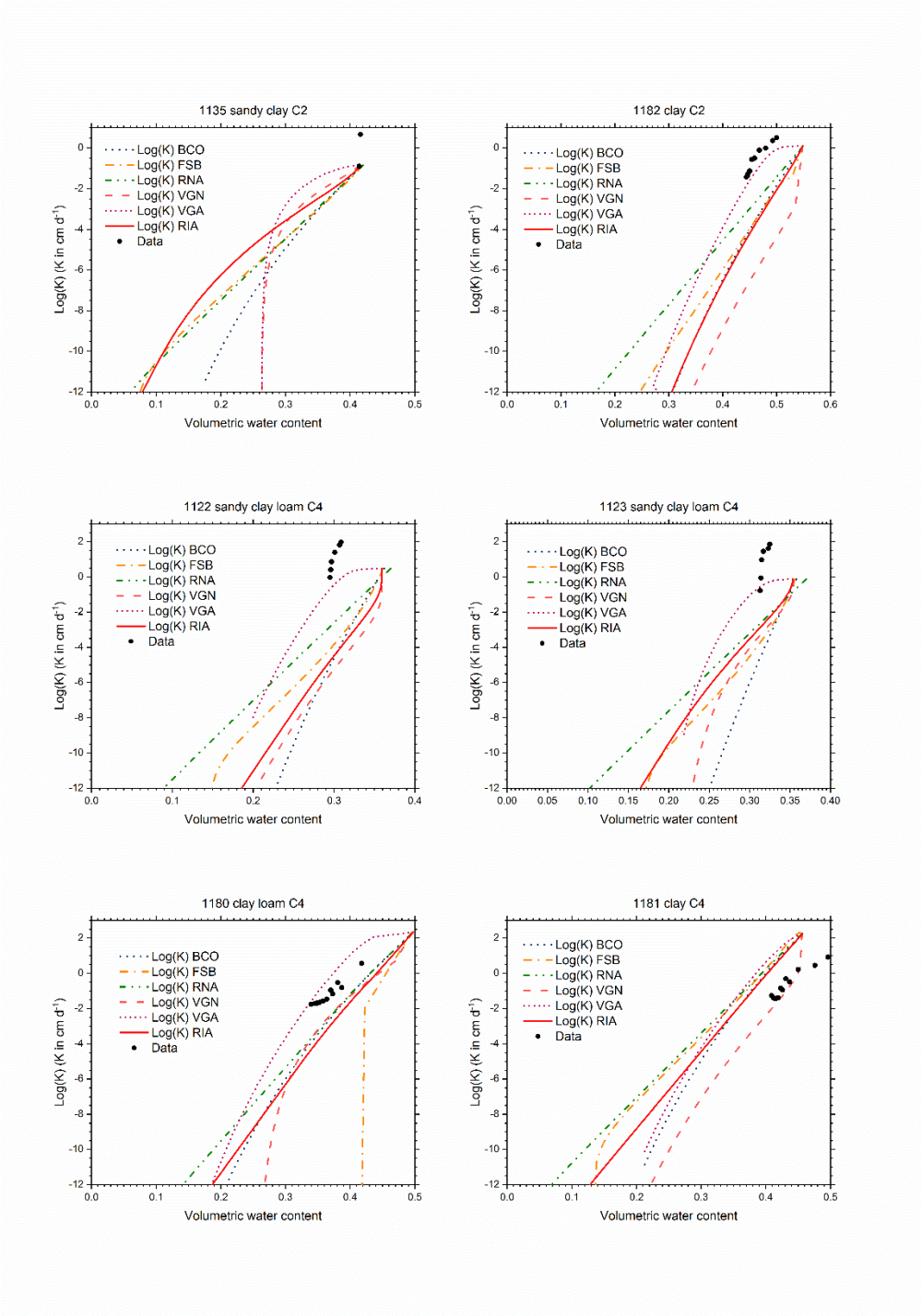

Figure C9. Conductivity data and conductivity curves derived from the retention curves of Fig. C5 according to six parameterizations for selected UNSODA soils with Twarakavi et al.'s (2010) C2 or AC4 classification.

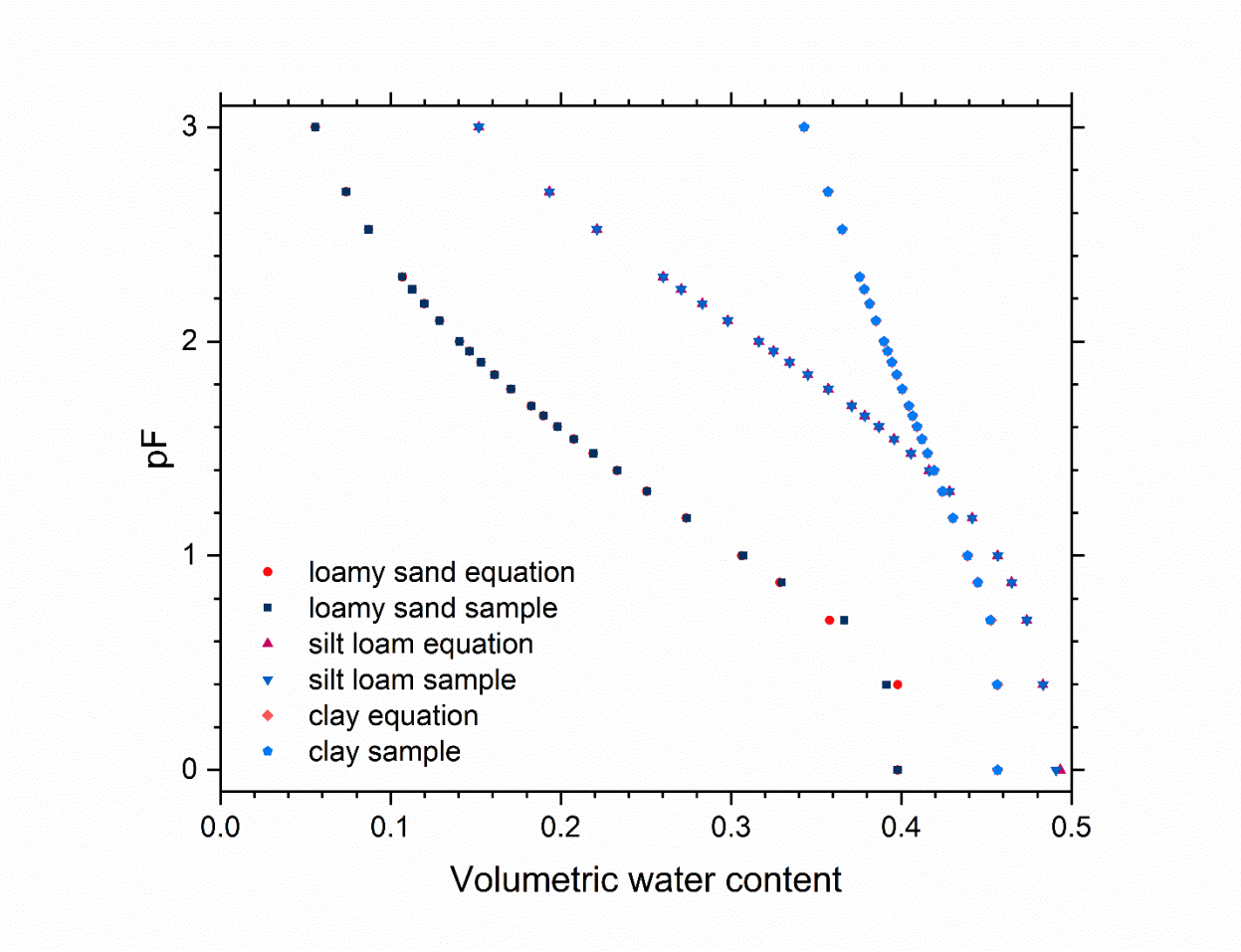

Figure C10. Soil water retention points calculated from RIA parameterizations for loamy sand (UNSODA identifier 2104, classification according to Twarakavi et al. (2010) A4), silt loam (3261, B2), and clay (1181, C4). The points were either calculated directly for the given pF value ('equation'), or by calculating the average water content in a sample of 5.0 cm height at hydrostatic equilibrium, with the matric potential at the center of the sample corresponding to the indicated pF value ('sample'). N.B. The data points for zero matric potential were plotted at $\mathrm{pF} = 0$ instead of $\mathrm{pF} = -\infty$.

Author contributions

GdR developed the new parameterization, assisted by RM. GdR identified the 21 soils from the UNSODA database and designed the model test. JM developed the SCE code for parameter identification. GdR coded the shell around the SCE core to make it suitable for fitting various SWRC parameterizations. GdR collected the weather data and generated the weather records. GdR and RM carried out the paramter fitting and the Hydrus–1D simulations. GdR wrote the manuscript with contributions from JM and RM.

Competing interests

GdR is a member of the HESS Editorial Board.

References

Assouline, S., and Or, D.: Conceptual and parametric representation of soil hydraulic properties: a review, Vadose Zone J., doi: 10.2136/vzj2013.07.0121, 2013.

Assouline, S., Tessier, D., and Bruand, A.: A conceptual model of the soil water retention curve, Water Resour. Res., 34, 223–231, 1998.

Bittelli, M., and Flury, M.: Errors in water retention curves determined with pressure plates, Soil Sci. Soc. Am. J., 73, 1453–1460, doi: 10.2136/sssaj2008.0082, 2009.

Bradley, R. S.: Polymolecular adsorbed films. Part 1. The adsorption of argon on salt crystals at low temperatures, and the determination of surface fields, J. Chem. Soc. (Resumed), 1467–1474, doi: 10.1039/JR9360001467, 1936.

Brooks, R. H., and Corey, A. T.: Hydraulic properties of porous media, Hydrology Paper No. 3, Colorado State University, 1964.

Campbell, G. S., and Shiozawa, S.: Prediction of hydraulic properties of soils using particle–size distribution and bulk density data, in: Proceedings of the international workshop on indirect methods for estimating the hydraulic properties of unsaturated soils, Riverside, California, Oct. 11–13, 1989, edited by: van Genuchten, M. Th., Leij, F. J., and Lund, L. J.editors, Univ. California, Riverside, CA, U.S.A., 317–328, 1992.

Cornelis, W. M., Khlosi, M., Hartmann, R., Van Meirvenne, M., and De Vos, B.: Comparison of unimodal analytical expressions for the soil–water retention curve, Soil Sci. Soc. Am. J. 69, 1902–1911, doi: 10.2136/sssaj2004.0238, 2005.

Durner, W.: Hydraulic conductivity estimation for soils with heterogeneous pore structure, Water Resour. Res., 30, 211–223, 1994.

712 Fayer, M. J., and Simmons, C. S.: Modified soil water retention function for all matric
713 suctions, Water Resour. Res., 31, 1233–1238, 1995.
714 Fredlund, D. G., and Xing, A.: Equations for the soil–water characteristic curve, Can. Geotech.
715 J., 31, 521–532, 1994.
716 Fuentes, C., Haverkamp, R., Parlange, J. –Y., Brutsaert, W., Zayani, K., and Vachaud, G.:
717 Constraints on parameters in three soil–water capillary retention functions,
718 Transport in Porous Media, 6, 445–449, 1991.
719 Hillel, D.: Environmental soil physics, Academic Press, San Diego, CA, U.S.A., 1998.
720 Hutson, J. L. and Cass, A.: A retentivity function for use in soil-water simulation models, J. of
721 Soil Sci., 38, 105–113, 1987.
722 Iden, S. C., Peters, A., and Durner, W.: Improving prediction of hydraulic conductivity by
723 constraining capillary bundle models to a maximum pore size, Adv. Water Resour.
724 85, 86–92, doi: 10.1016/j.advwatres, 2015.09.005, 2015.
725 Ippisch, O., Vogel, H. –J., and Bastian, P.: Validity limits for the van Genuchten–Mualem
726 model and implications for parameter estimation and numerical simulation, Adv.
727 Water Resour., 29, 1780–1789, doi: 10.1016/j.advwatres.2005.12.011, 2006.
728 Khlosi, M., Cornelis, W. M., Douaik, A., van Genuchten, M. Th., and Gabriels. D.: Performance
729 evaluation of models that describe the soil water retention curve between saturation
730 and oven dryness, Vadose Zone J., 7, 87–96, doi: 10.2136/vzj2007.0099, 2008.
731 Khlosi, M., Cornelis, W. M., Gabriels, D., and Sin, G.: Simple modification to describe the soil
732 water retention curve between saturation and oven dryness, Water Resour. Res., 42,
733 W11501, doi: 10.1029/2005WR004699, 2006.

734 Klute, A.: Water retention: Laboratory methods, in: Methods of soil analysis. Part 1. Physical
735 and mineralogical methods. Second edition, edited by Klute, A., American Society of
736 Agronomy, Inc., Soil Science Society of America, Inc., Madison, WI, U.S.A., 635–662,
737 1986.
738 Kool, J. B., and Parker, J. C.: Development and evaluation of closed–form expressions for
739 hysteretic soil hydraulic properties, Water Resour. Res., 23, 105–114, 1987.
740 Koorevaar, P., Menelik, G., and Dirksen, C.: Elements of soil physics, Elsevier, Amsterdam,
741 The Netherlands, 1983.
742 Kosugi, K.: General model for unsaturated hydraulic conductivity for soils with lognormal
743 pore–size distribution, Soil Sci. Soc. Am. J., 63,270–277, 1999.
744 Kroes, J. G., van Dam, J. C., Bartholomeus, R. P., Groenendijk, P., Heinen, M., Hendriks, R. F. A.,
745 Mulder, H. M., Supit, I., and van Walsum, P. E. V.: SWAP version 4. Theory description
746 and user manual, Report 27480, Wageningen Environmental Research, Wageningen,
747 The Netherlands, 244 pp, doi: 10.18174/416321, 2017.
748 Leij, F. J., Russell, W. B., and Lesch, S. M.: Closed–form expressions for water retention and
749 conductivity data, Ground Water, 35, 848–858, 1997.
750 Liu, H. H., and Dane, J. H.: Improved computational procedure for retention relations of
751 immiscible fluids using pressure cells, Soil Sci. Soc. Am. J., 59, 1520–1524, 1995.
752 Madi, R., de Rooij, G. H., Mielenz, H., and Mai, J.: Parametric soil water models: a critical
753 evaluation of expressions for the full moisture range, Hydrol. Earth Syst. Sci. 22,
754 1193–1219, doi: 10.5194/hess-22-1193-2018, 2018.
755 Mualem, Y.: A new model for predicting the hydraulic conductivity of unsaturated porous
756 media, Water Resour. Res., 12, 513–522, 1976.

National Agricultural Library, UNSODA Database, https://data.nal.usda.gov/dataset/unsoda-20-unsaturated-soil-hydraulic-database-database-and-program-indirect-methods-estimating-unsaturated-hydraulic-properties_134, last access 22 July 2020.

Nemes, A., Schaap, M. G., Leij, F. J., and Wösten, J. H. M.: Description of the unsaturated soil hydraulic database UNSODA version 2.0., J. Hydrol., 251, 152–162, doi: 10.1016/S0022-1694(01)00465-6, 2001.

PC-progress: https://www.pc-progress.com/en/Default.aspx?hydrus-1d, last access: 22 July 2020.

Peters, A.: Simple consistent models for water retention and hydraulic conductivity in the complete moisture range, Water Resour. Res., 49, 6765–6780, doi: 10.1002/wrcr.20548, 2013.

Peters, A., Durner, W., and Wessolek, G.: Consistent parameter constraints for soil hydraulic functions, Adv. Water Resour., 34, 1352–1365, doi: 10.1016/j.advwatres.2011.07.006, 2011.

Rossi, C., and Nimmo. J. R.: Modeling of soil water retention from saturation to oven dryness, Water Resour. Res., 30, 701–708, 1994.

Rudiyanto, Minasny B., Shah, R. M., Setiawan, B. I., and van Genuchten, M. Th.: Simple functions for describing soil water retention and the unsaturated hydraulic conductivity from saturation to complete dryness, J. Hydrol., 588, 125041, doi: 10.1016/j.jhydrol.2020.125041, 2020.

778 Schaap, M. G., and van Genuchten, M. Th.: A modified Mualem–van Genuchten formulation
779 for improved description of the hydraulic conductivity near saturation, Vadose Zone
780 J. 5, 27–34, doi: 10.2136/vzj2005.0005, 2006.
781 Schneider, M, and Goss, K. –U.: Prediction of the water sorption isotherm in air dry soils,
782 Geoderma, 170, 64–69, doi: 10.1016/j.geoderma.2011.10.008, 2012.
783 Šimůnek, J., and Bradford, S. A.: Vadose zone modeling: Introduction and Importance,
784 Vadose Zone J., 7, 581–586, doi: 10.2136/vzj2008.0012, 2008.
785 Šimůnek, J., Šejna, M., Sait., H., Sakai, M., and van Genuchten, M. Th.: The HYDRUS–1D
786 software package for simulating the one–dimensional movement of water, heat, and
787 multiple solutes in variably–saturated media, Version 4.17, Dept. Env. Sci., Univ.
788 Calif., Riverside, CA, U.S.A., 2013.
789 Šimůnek, J, van Genuchten, M. Th., and Šejna, M.: Recent developments and applications of
790 the HYDRUS computer software packages, Vadose Zone J., doi:
791 10.2136/vzj2016.04.0033, 2016.
792 Twarakavi, N. K. C., Šimůnek, J., and Schaap, M. G.: Can texture–based classification
793 optimally classify soils with respect to soil hydraulics?, Water Resour. Res. 46,
794 W01501, doi:10.1029/2009WR007939, 2010.
795 van Genuchten, M. Th.: A closed–form equation for predicting the hydraulic conductivity for
796 unsaturated soils, Soil Sci. Soc. Am. J., 44, 892–898, 1980.
797 Vogel, T., van Genuchten, M. Th., and Cislerova, M.: Effect of the shape of the soil hydraulic
798 functions near saturation on variably–saturated flow predictions, Adv. Water
799 Resour., 24, 133–144, 2001.

Wang, Y., Jin, M., and Deng, Z.: Alternative model for predicting soil hydraulic conductivity over the complete moisture range, Water Resour. Res., 54, 6860–6876, doi: 10.1029/2018WR023037, 2018.

Wang, Y., Ma, J., and Huade, G.: A mathematically continuous model for describing the hydraulic properties of unsaturated porous media over the entire range of matric suctions. J. Hydrol,. 541, 873–888, doi: 10.1016/j.jhydrol.2016.07.046, 2016.

Weber, T. K. D., Durner, W., Streck, T., and Diamantopoulos, E.: A modular framework for modeling unsaturated soil hydraulic properties over the full moisture range, Water Resour. Res., 55, doi: 10.1029/2018WR024584, 2019.

Zurmühl, T., and Durner, W.: Determination of parameters for bimodal hydraulic functions by inverse modeling, Soil Sci. Soc. Am. J., 62, 874–880, 1998.